
Politecnico di Torino

**POLITECNICO DI TORINO**

MSc. Environmental and Land Engineering
Graduation session November 2025
Academic Year 2024/25

# Flood disaster management using Earth Observation technologies

Supervisors:

Prof. Piero Boccardo
Sona Guliyeva

Candidate:

Hossein TaheriJafari

# Abstract

Floods are among the most frequent and damaging disasters worldwide, affecting millions of people and causing high economic losses. Traditional ground-based monitoring systems often lack sufficient coverage, particularly in vulnerable regions, creating a need for more reliable tools. Satellite-based Earth Observation (EO) has emerged as a vital resource for flood detection, monitoring, and management. Satellites including Sentinel-1, Sentinel-2, Landsat, and commercial constellations like Planetscope, Skysat, COSMO-SkyMed provide valuable datasets to map inundation, assess damage, and guide emergency response.

This thesis focuses on the Emilia-Romagna floods of May 2023, one of the most severe in recent decades in Italy, particularly in Spazzate-Sassatelli. Using Sentinel-2 (open-source) and SkySat (commercial) imagery, a modular Python-based algorithm was developed to process images based on K-means clustering machine learning method. Results showed that algorithm for Sentinel-2 could generate regional maps in less than one minute using cloud-based processing such as Google colab, while algorithm for SkySat provided finer-scale details within ~4 minutes on local hardware. Accuracy assessments confirmed Sentinel-2's effectiveness at large scales, although SkySat offered superior precision in urban and narrow floodplain contexts. The Sentinel-2 algorithm offers cleaner and more precise flood detection, while SkySat identifies a wider area but with slightly more false positives. Overall, both deliver comparable performance.

Overall, free open data is good for making fast maps of small areas, while very detailed commercial images are better for showing local damage clearly besides efficient result for large area. In the future, flood monitoring should use more automation, machine learning, and real-time systems to respond faster and more effectively.

# Table of contents

# Introduction

**Background: importance of flood monitoring and management**

Floods are among the most destructive and frequent natural hazard worldwide, with profound social, environmental, and economic consequences. According to the International Disaster Database, floods represent the most common type of weather-related disaster, affecting more people than any other natural hazard. Between 2006 and 2015, an estimated 800 million individuals were impacted by flood events, and the total economic damage exceeded $300 billion globally. These figures highlight the urgent need for effective flood monitoring and management strategies [1].

Despite growing awareness of the ecological and societal importance of river systems and their inundation dynamics, the capacity to accurately model and predict flood events remains limited. This is largely attributed to the scarcity of consistent, high-resolution in-situ measurements, particularly in remote regions and developing countries. Traditional ground-based monitoring infrastructure, such as gauging stations and field surveys, has declined in coverage and quality, creating critical data gaps in many vulnerable areas. [1].

In response to these challenges, remote sensing has emerged as a valuable and increasingly indispensable tool for flood observation and analysis. Satellite-based sensors provide spatially continuous and temporally frequent datasets that can capture key variables such as terrain elevation, river width, flood extent, water levels, and land cover. When integrated into hydrological and hydraulic models, these datasets significantly enhance the understanding and forecasting of flood dynamics. This is particularly beneficial for data-scarce catchments, where traditional measurements are unavailable or unreliable [1].

Furthermore, advancements in remote sensing technologies have enabled the development of global datasets for parameters such as precipitation, evapotranspiration, temperature, and land use. These datasets are critical for modelling flood behavior in ungauged or sparsely gauged basins. For instance, demonstrated the successful use of remote sensing products to generate flood inundation maps for the large-scale, poorly monitored Brahmaputra Basin, underscoring the practical applicability of such tools in flood-prone regions [2].

# Description of the Study Area

**Emilia Romagna overview**

In May 2023, was the hardest rain fall event that estimated once every 200 years. This event had two major intense rainfall, in the early May and in mid-May that was more intense and because of second event the inundated area exacerbated. On April 20, 2023, Civil Protection issued an orange alert (moderate risk) for thunderstorms in Emilia-Romagna. A few days later, on April 24 and 25, heavy rain and hail hit several provinces, including Ferrara, Parma, Reggio-Emilia, and Rimini. The strongest rainfall began on May 2, leading to a red alert within 12 hours. In just two days, 200 mm of rain fell in Bologna, Ravenna, and Forlì-Cesena, mostly affecting the Romagna area, which caused rivers to overflow and widespread flooding. By May 4, 23 rivers had overflowed, 15 levees had broken, more than 140 landslides had occurred, and there was serious damage to infrastructure. The situation worsened with more rainfall on May 9 and 10. On May 16 and 17, rain reached record levels again, with 300 mm in Forlì and up to 200 mm in Ravenna and Bologna. By May 18, around 8,000 volunteer workdays had been dedicated to managing the disaster, and a 12-month state of emergency was declared. Before May 25, 23 rivers had overflowed, 13 had reached critical levels, and the floods caused 50 incidents across 42 municipalities. In addition, more than 370 landslides blocked over 700 roads. By May 20, the disaster had forced 36,600 people to evacuate and caused 17 deaths, most of them elderly.[3]

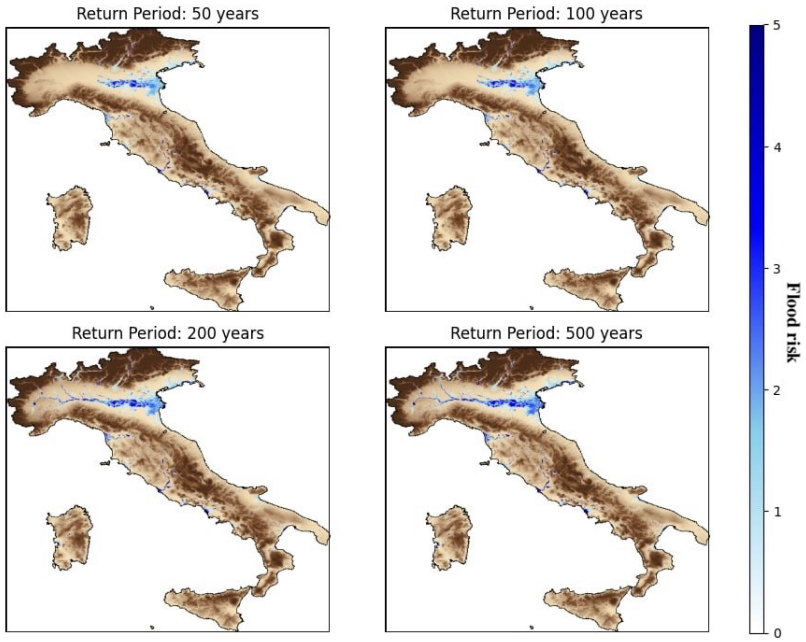


Figure 1 Flood risk in Italy

# Area of interest: Spazzate-Sassatelli

The rising rivers quickly created dangerous conditions, with the Sillaro River embankment breaking and the Lamone River overflowing, flooding areas near Massa Lombarda and Conselice. In response, the Copernicus Emergency Management Service (EMS) Rapid Mapping was activated to provide early estimates of flood extent and damage. As part of this activation (EMSR659), a detailed impact assessment was carried out in the Spazzate-Sassatelli area. The analysis showed that around 1,610.9 hectares of land were submerged, with flood traces covering an additional 20.8 hectares. [4]

Approximately 200 people were affected, out of a local population of about 16,000. The built environment suffered moderate damage, mainly to housing. Of 6,568 residential buildings, 250 were impacted, one was destroyed, 130 were damaged, and 119 were possibly damaged. Other structures, including industrial, commercial, and religious buildings remained largely unaffected, showing the localized nature of the flooding. Transport infrastructure faced selective impacts. Major roads were not destroyed, but smaller routes suffered. 26.9 km of cart tracks were flooded, with 18.3 km damaged, while local roads recorded about 1.9 km of confirmed or possible damage due to flooding and washouts. Public facilities saw minor effects, with 9.8 hectares of sports and recreation areas affected out of a total of 21.6 hectares. [4]

No damage was reported to energy, communication, or pipeline networks. Agriculture, however, faced significant losses. About 1,319.3 hectares of arable land were flooded, over 10% of the cultivated area, while 182.2 hectares of permanent crops, such as orchards and vineyards, were inundated, raising concerns for long-term productivity. Inland wetlands and mixed-use agricultural zones also showed some damage.[4]

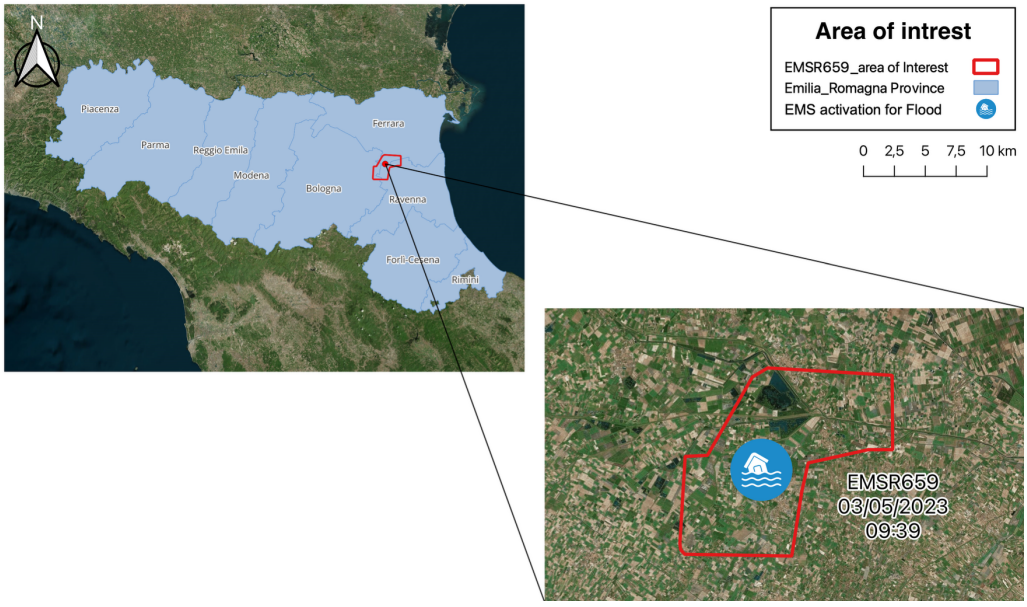


Figure 2 Area of interest

| Consequences within the AOI | | | | |
|---|---|---|---|---|
| | Unit of measurement | | Affected | Total in AOI |
| Flooded area | | ha | | 1,316.3 |
| Estimated population | Number of inhabitants | | ~ 200 | ~ 7,400 |
| Built-up | Residential Buildings | No. | 139 | 2,900 |
| | Industrial buildings | No. | 18 | 161 |
| | Buildings used as places of worship and for religious activities | No. | 1 | 6 |
| | Communication buildings, stations, terminals and associated buildings | No. | 0 | 1 |
| Transportation | Airfield runways | km | 0.3 | 0.5 |
| | Primary Road | km | 0.0 | 10.2 |
| | Secondary Road | km | 1.9 | 12.0 |
| | Local Road | km | 1.7 | 47.0 |
| | Cart Track | km | 16.9 | 117.9 |
| | Long-distance railways | km | 0.0 | 6.7 |
| Facilities | Sport and recreation constructions | ha | 6.4 | 19.6 |
| | Long-distance pipelines, communication and electricity lines | km | 4.2 | 38.4 |
| | Local pipelines and cables | km | 0.0 | 0.3 |
| Land use | Arable land | ha | 1,066.6 | 6,156.0 |
| | Permanent crops | ha | 149.4 | 219.1 |
| | Heterogeneous agricultural areas | ha | 90.3 | 1,481.5 |
| | Other | ha | 10.0 | 201.1 |

**Table 1 Impact statistics (from EMSR659)** [4]

# Why this area is suitable for analysis

The Emilia-Romagna region has been selected because it has experienced frequent and severe flood events, especially between 2012 and 2025 in Italy. These repeated disasters make it an important case study for understanding monitoring of flood. The figure presented here illustrates the number of activations and products generated by the Copernicus Emergency Management Service (CEMS) specifically for Emilia-Romagna. In other words, it shows how often the region has required rapid mapping support during floods and how much geospatial information was produced to assist emergency response and recovery. This repeated need for CEMS products highlights both the vulnerability of the area and its importance in studying flood monitoring and management.

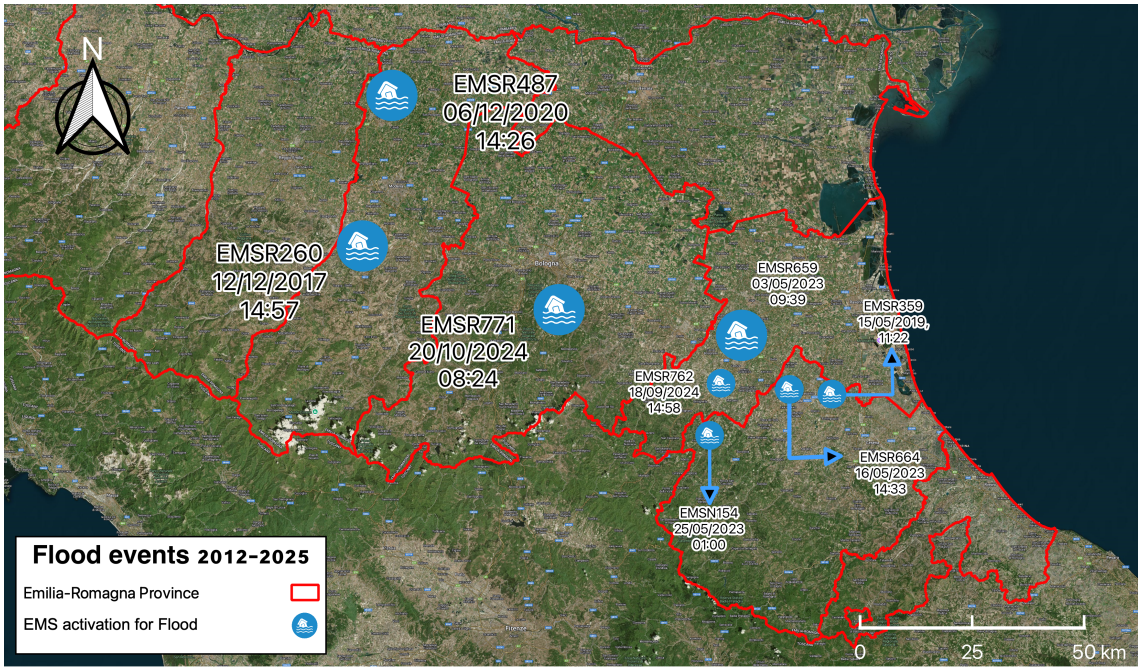


Figure 3 flood events by EMS

Spazzate-Sassatelli sits on the active Sillaro floodplain, experienced repeated inundation in May 2023, and is covered by Copernicus, Skysat and UVA products and detailed local records, exactly the combination is demanded for robust flood detection analysis, mapping accuracy and timing exposure.

# Objectives of the Study

- To explore methods for reducing the time needed to produce reliable flood maps.

- To evaluate suitable machine learning method for detecting the desire data as water layer.

- To assess the differences between Sentinel-2 (open-source) and SkySat (commercial) imagery in terms of accuracy, detail, and processing time in results of each created algorithm.

- To design and test workflows and frameworks that can deliver flood maps more quickly and efficiently.

# Background and Literature Review

**Overview of remote sensing in flood detection and management.**

## Remote Sensing for Flood Management

### Historical and Current State

Satellite technology has played an important role in disaster management since the late 1950s. After the launch of the first U.S. satellite, Explorer 1, in 1958, satellites were first used to monitor weather. By the late 1980s, satellite images started to help with disaster response, such as during Hurricane Hugo in 1989[5]. In the 1990s, the growth of Geographic Information Systems (GIS) made it much easier to use satellite data for many purposes, including managing natural disasters[6]; [7]; [8]. For example, in 1992, NASA sent images to Hawaii after Hurricane Iniki to help with the response. In 1993, satellite images were also used by government agencies like Federal Emergency Response Agency (FEMA) and the U.S. Army Corps of Engineers to respond to the Great Midwest Flood. These images helped create maps, monitor how the flood was spreading, and check for damage to farms and infrastructure. This success led FEMA to support more work on using satellites for future flood response [5].

To improve coordination between space agencies and disaster response teams, the United Nations started the International Charter: Space and Major Disasters in 2000 [9]; [10]. Since then, many organizations, including the European Union's Copernicus program, NASA, NOAA, and the U.S. Geological Survey, have used satellite data to help with

disaster response. These efforts are now supported by international cooperation through the UN Office for Outer Space Affairs (UN-OOSA)[11].

Earth observation has become a vital tool in all stages of flood management. Satellite remote sensing provides timely, large-scale data for monitoring floods and assessing impacts when ground observations are sparse or disrupted. By capturing inundation extents, rainfall estimates, and terrain information from space, remote sensing supports better preparedness, real-time flood mapping for emergency response, and post-event damage evaluation. It effectively complements in-situ gauge networks, which in Europe are not uniformly distributed, helping to “fill the gap” in flood observation. In recent years, advances in sensors and data processing (e.g. the European Copernicus program) have greatly enhanced the ability to detect and manage floods from space [11][12].

In this section the primary remote sensing technologies and sensor types used to detect and map floods reviewed.

# EO Sensors and Platforms

Remote sensing is the science of acquiring information about the Earth's surface without direct physical contact, typically through sensors mounted on satellites or airborne platforms. These systems are broadly categorized into active and passive sensors, based on their dependence on external energy sources [13]; [14].

Passive remote sensing relies on natural energy, primarily sunlight, which is either reflected or emitted by the Earth's surface and captured by the sensor. Common passive sensors operate in the visible, near infrared, and thermal infrared regions of the electromagnetic spectrum. Satellite missions such as Landsat, MODIS, and Sentinel-2 utilize passive sensing for applications including land cover classification, vegetation monitoring, and thermal mapping. However, passive systems are limited by the availability of natural light and are often ineffective under cloudy conditions or at night [13]

In contrast, active remote sensing systems release their own energy toward the target and record the reflected signal. This capability allows them to operate independently of sunlight and penetrate atmospheric conditions like clouds and rain. Radar (e.g., SAR) and LiDAR are typical examples of active sensors. Active remote sensing is especially valuable for terrain modeling, surface deformation monitoring, and structural analysis, due to its ability to capture high-resolution and geometrically precise data regardless of weather or lighting [15], [16]

The distinction between active and passive sensors is fundamental for selecting appropriate remote sensing techniques, as each has its strengths and limitations depending on the application and environmental conditions.

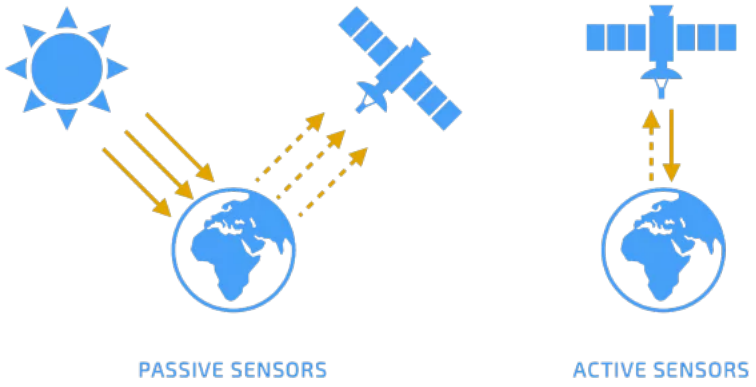


**Figure 4 illustration of active and passive sensors**

Electromagnetic (EM) waves are a form of energy propagation consisting of oscillating electric and magnetic fields that are perpendicular to each other and the direction of wave propagation. First described by James Clerk Maxwell in the 19th century, these waves travel through space at the speed of light, approximately $3 \times 10^8$ m/s. The waves are generated by the acceleration of charged particles, which create oscillating electric and magnetic fields that sustain each other as they propagate. This concept of EM wave propagation, with its fundamental principles, was first laid out by Maxwell in 1865 and later extended by other researchers, such as Ulaby, Moore, and Fung, who provided further insights into the wave's behavior and applications [17], [18].

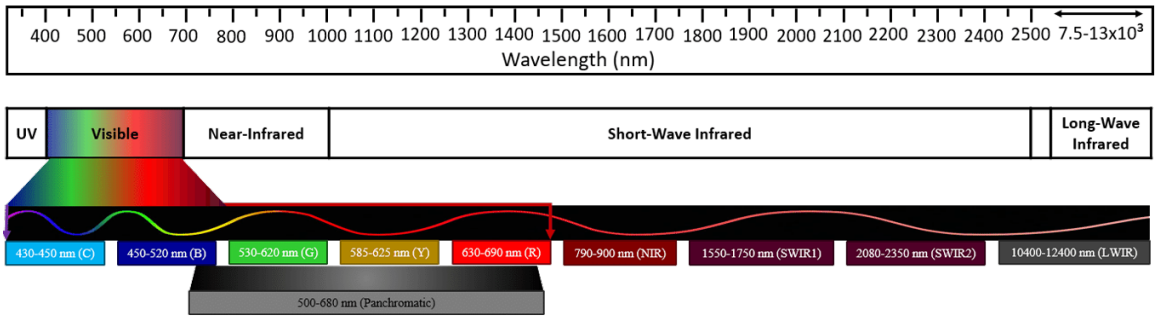


**Figure 5 Electromagnetic waves spectrum**

## Flood Detection Techniques

### Normalized Difference Water Index (NDWI)

The Normalized Difference Water Index (NDWI), which utilizes reflectance values from the green and near-infrared (NIR) bands, is designed to enhance the spectral distinction between water surfaces and terrestrial features in these spectral regions. It has been widely applied in flood mapping and surface water delineation across numerous studies. While several other water indices have been developed over time, NDWI has consistently demonstrated superior performance in identifying water bodies. The index produces values ranging from −1 to +1, with positive values typically indicating the presence of surface water, particularly in cases of deep and clear water. However, the effectiveness of NDWI can be compromised in areas with dense vegetation. In such environments, higher NIR reflectance compared to green reflectance may result in NDWI values resembling those of non-water land covers, making it more challenging to accurately delineate complex or diverse flooded landscapes.[19]

The NDWI is expressed as follow[20]

$$NDWI = \frac{Green - NIR}{Green + NIR}$$

The NDWI is designed to make water areas stand out more clearly in satellite images. It does this by using the green band, where water reflects a lot of light, and the near-infrared (NIR) band, where water reflects very little. At the same time, land surfaces like vegetation and soil reflect much more light in the NIR band. Because of this, water usually appears with positive NDWI values, making it easy to identify, while land areas have values close to zero or negative, which helps reduce their influence in the results.[20]

To remove the confusion caused by built-up areas in water detection, their unique reflectance characteristics need to be studied. Figure illustrated bellow shows how water of lake, vegetation, and built-up land reflect light across different bands. In the green band, spectral bands of the Landsat Thematic Mapper (TM2) and near-infrared (NIR) band (TM 4), built-up land reflects light in a similar way to water, both reflect more green light than NIR. Because of this, the NDWI gives positive values not only for water but also for built-up land, which can lead to false identification of water areas in NDWI results.[21]

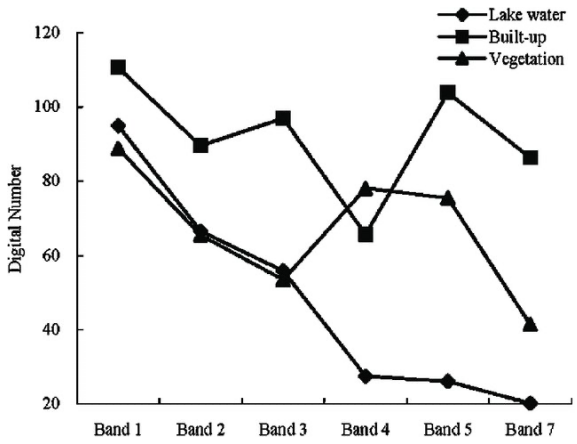


**Figure 6 spectral reflectance**[21]

However, when we look more closely at the spectral signatures, we see that the average reflectance of built-up land is much higher in the middle-infrared (MIR) band (TM 5) than in the green band (TM 2). So, if we replace the NIR band with the MIR band in the NDWI formula, built-up areas should show negative values, helping to separate them from water. This idea led to the creation of the Modified NDWI (MNDWI), which uses the MIR band instead of the NIR band.[21]

$$MNDWI = \frac{Green - MIR}{Green + MIR}$$

# SAR technology

Real Aperture Radar (RAR) is a traditional radar system that utilizes a physical antenna of fixed size to transmit and receive electromagnetic signals. The antenna's size is directly related to the radar's resolution specifically; the size of the antenna determines the resolution in the azimuth direction (across the direction of motion). In Real Aperture Radar (RAR), the radar transmits pulses and receives the reflected signals from objects on the ground, with the resolution in the range direction (along the line of sight) determined by the pulse duration and bandwidth. However, the main limitation of RAR is that improving the resolution requires increasing the physical size of the antenna, which is not practical, especially in space-based or airborne systems, where space and weight are constrained [18].

In contrast to RAR, Synthetic Aperture Radar (SAR) is a more advanced technology that limits the size of antennas by using the motion of the radar platform (such as a satellite or aircraft) to simulate a much larger antenna. The basic principle behind SAR is that, as the radar platform moves along its flight path, it continuously transmits pulses and receives echoes from the target area. These echoes, captured from multiple positions, are processed together to simulate a large virtual antenna, or "synthetic" aperture, significantly enhancing the azimuth resolution [22]

SAR relies on complex signal processing to combine the radar data collected from different points, allowing it to achieve high resolution despite the relatively small size of the physical antenna. This technique leverages Doppler shift and phase information from multiple radar echoes to achieve the desired resolution, which is not limited by the physical size of the antenna[23]

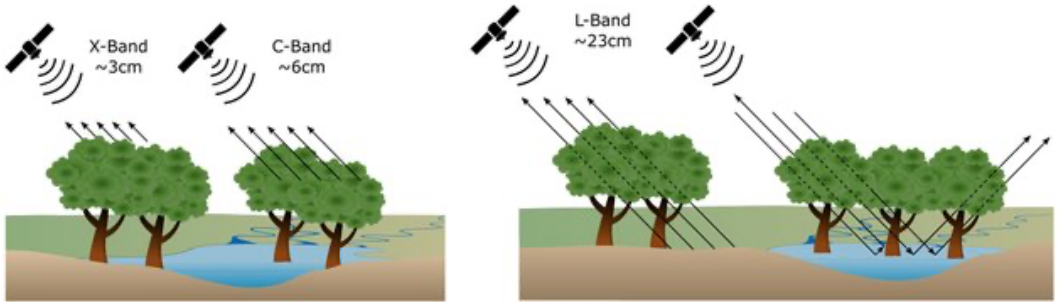


**Figure 7 Radar backscattering mechanisms for different SAR wavelengths: X- and C-band (top) and L-band (bottom).[39]**

## Global Operational SAR Satellites (2025)

| Satellite / Mission | Operator / Agency | Frequency Band | Spatial Resolution | Revisit Time | Data Accessibility |
|---|---|---|---|---|---|
| **Sentinel-1A** | ESA (EU) | C-band | ~5 m (Stripmap mode) | ~12 days (6 days with 2 sats) | Public (open data) |
| **TerraSAR-X & TanDEM-X** | DLR/Airbus (Germany) | X-band | up to 0.25 m (Spotlight) | 11 days (exact repeat) | Commercial (Airbus) |
| **PAZ** | Hisdesat (Spain) | X-band | ~1 m (Spotlight) | 11 days | Commercial (Airbus/Hisdesat) |
| **COSMO-SkyMed (1st Gen – 4 sats)** | ASI/Italian MoD (Italy) | X-band | ~1 m (Spotlight) | <1 day | Commercial & Military |
| **COSMO-SkyMed (2nd Gen – 2 sats)** | ASI/Italian MoD (Italy) | X-band | ~0.8 m (Spotlight) | ~1–2 days | Commercial & Military |
| **RADARSAT-2** | CSA/MDA (Canada) | C-band | 1 m (Spotlight mode) | 24 days | Commercial |
| **RADARSAT Constellation (RCM)** | CSA (Canada) | C-band | ~3 m (Stripmap); 1×3 m Spotlight | ~4 days | Public |
| **ALOS-2 (Daichi-2)** | JAXA (Japan) | L-band | 1×3 m (Spotlight) | 14 days | Restricted |
| **SAOCOM-1A/1B** | CONAE (Argentina) | L-band | ~10 m (Stripmap) | 8 days | Public for research |
| **NovaSAR-1** | SSTL/CSIRO (UK/Australia) | S-band | 6 m (Stripmap) | ~3–4 days | Commercial |
| **KOMPSAT-5** | KARI (South Korea) | X-band | 1 m (Spotlight) | 28 days | Commercial |
| **Gaofen-3** | CNSA (China) | C-band | ~1 m (Spotlight mode) | 29 days | Restricted |

| | | | | | |
|---|---|---|---|---|---|
| **Huanjing-2E** | MEE/CNSA (China) | S-band | 5 m (resolution) | ~60-day coverage | Restricted |
| **L-SAR 01A/B** | CNSA (China) | L-band | ~5 m (high-res mode) | ~8 days | Restricted |
| **ICEYE** | ICEYE (Finland) | X-band | 0.25 m (Spotlight) | Hours | Commercial |
| **Capella Space** | Capella Space (USA) | X-band | ~0.5 m (Spotlight) | Hours | Commercial |
| **Umbra** | Umbra Space (USA) | X-band | 0.25 m (Spotlight) | ~4 per day | Commercial |
| **Synspective StriX** | Synspective (Japan) | X-band | ~1 m (Spotlight) | Days | Commercial |
| **iQPS (QPS-SAR)** | iQPS (Japan) | X-band | ~0.75 m (Spotlight) | Days | Commercial |
| **Hisea-1** | Spacety (China) | C-band | 1 m (Stripmode) | ~15 days | Commercial |

**Table 2 Open source and Commercial SAR Satellites**

## Optical and Multispectral Imaging (passive sensor)

Optical satellites (e.g. Sentinel-2, Landsat 8/9) capture reflected sunlight in visible and infrared bands, providing detailed images of inundation extent in clear conditions. These sensors offer high spatial detail (10–30 m resolution) and rich spectral information to distinguish water from land. Multispectral imagery has successfully been used to map floods before, during, and after events, including using infrared bands to enhance water detection. Very-high-resolution optical data from commercial satellites (e.g. SPOT, Worldview) have even been employed for detailed urban flood assessments[1].
Optical remote sensing (e.g., visible and near-infrared bands) provides familiar photographic-like imagery of floods. Multispectral satellites capture reflectance in several bands, enabling the use of spectral indices to identify water. Water has strong absorption in near-infrared and shortwave infrared wavelengths, making flooded areas standout (often as dark or blueish areas in false-color composites). Common water indices include the Normalized Difference Water Index (NDWI) and its variants (e.g., MNDWI), which emphasizes open water by combining green, NIR, or SWIR bands[12].

### Operational Optical Earth Observation Satellites (as of 2025)

This table presents a comprehensive overview of currently operational optical Earth observation satellites, categorized by spatial resolution: very high, high, and medium. Each table entry includes the satellite name (or constellation), spatial resolution, revisit frequency (temporal resolution), launch year, operator, and data accessibility.

| Satellite (Launch) | Spatial Resolution | Revisit Frequency | Operator | Data Access |
|---|---|---|---|---|
| **WorldView-3 (2014)** | 0.31 m pan; 1.24 m multispectral (VHR) | On-demand (daily possible) | Maxar (USA) | Commercial |

| | | | | |
|---|---|---|---|---|
| **WorldView-2 (2009)** | 0.46 m pan; 1.84 m MS | ~1.1 days | Maxar (USA) | Commercial |
| **SkySat Constellation (2016–2020)** | 0.50 m pan | Up to 10× daily | Planet Labs (USA) | Commercial |
| **Pléiades Neo (2021)** | 0.30 m pan; 1.2 m MS | ~2× daily | Airbus (France) | Commercial |
| **BlackSky Gen-3(2025)** | 35 cm, (NIIRS-5+) | < 10 hours | BlackSky (USA) | Commercial |
| **Jilin-1 Constellation (2015– )** | ~0.50–0.75 m pan | Up to ~6× daily | CGSTL (China) | Commercial |
| **SuperView Neo-1 (2022–2025)** | 0.30 m pan; 1.2 m MS (VHR) | Daily (with ~4 sats planned; intraday possible) | Siwei (China) | Commercial |
| **GeoEye-1 (2008)** | 0.41 m pan; 1.65 m MS (VHR) | ~3 days (with pointing; part of Maxar constellation) | Maxar (USA) | Commercial |
| **WorldView Legion (2024)** | 0.30 m pan (VHR) | Up to 15× per day (with 6-sat constellation) | Maxar (USA) | Commercial |
| **Cartosat-3 (2019)** | 0.25–0.3 m pan; ~1 m MS (VHR) | ~<5 days (agile single satellite) | ISRO (India) | Govt./Commercial |
| **Satellogic Aleph-1 (2016– )** | ~0.70 m pan (VHR) | ~4× per day (with ~17 sats) | Satellogic (Argentina) | Commercial |
| **EROS-C3 (2022)** | 0.38 m pan; 0.76 m MS (VHR) | On-demand (sub-daily tasking, part of EROS constellation) | ImageSat (Israel) | Commercial |
| **Göktürk-1 (2016)** | 0.50 m pan; 2 m color (VHR) | ~Daily (sun-sync; ~0.5 m GSD globally) | MoD (Turkey) | Govt./Commercial |
| **KhalifaSat (2018)** | ~0.70 m pan (VHR) | ~3 days (sun-sync orbit) | MBRSC (UAE) | Govt./Commercial |
| **PerúSAT-1 (2016)** | 0.70 m pan; 2 m MS (VHR) | ~Daily (sun-sync, taskable) | CONIDA (Peru) | Govt./Commercial |

**Table 3 Very High Resolution (sub-meter) Satellites**

These satellites have high spatial resolution on the order of a few meters (up to ~10 m), suitable for detailed mapping over large areas.

| Satellite (Launch) | Spatial Resolution | Revisit Frequency | Operator | Data Access |
|---|---|---|---|---|
| **PlanetScope (Dove) Constellation (2014)** | ~3 m multispectral (high) | Daily global (near all land, >430 CubeSats) | Planet Labs (USA) | Commercial |
| **Sentinel-2A/2B (2015/2017)** | 10 m (visible/NIR), 20 m & 60 m bands (high) | 5 days (global, 2-sat constellation) | ESA/EU (Copernicus) | Open (Free) |
| **Landsat 8 & 9 (2013/2021)** | 15 m pan; 30 m multispectral (high) | 8 days (global, with both; 16 days each) | NASA/USGS (USA) | Open (Free) |
| **Resourcesat-2/2A (2011/2016)** | 5.8 m pan; 23 m multispectral (high) | ~5 days (with 2 satellites) | ISRO (India) | Govt./Commercial[1] |
| **Gaofen-1 / -6 (2013/2018)** | 2 m pan; 8 m MS (high) | ~4 days (with multisat wide swath) | CNSA (China) | Govt./Commercial[1] |
| **CBERS-4 / 4A (2014/2019)** | 2–5 m pan; 8–10 m MS (high) | ~3–4 days (multiple cameras) | INPE/CNSA (Brazil/China) | Open (Free) |
| **VNREDSat-1 (2013)** | 2.5 m pan; 10 m MS (high) | ~3 days (sun-sync orbit) | VAST (Vietnam) | Govt./Commercial |
| **RapidEye (2008) – Retired 2020** | 5 m multispectral (high) | Daily (5-sat constellation) | Planet (Germany) | Open (Free)[2] |

**Table 4 High Resolution (meter-level) Satellites**

[1] Restricted-access data (not freely available to the public).
[2] Rapid Eye imagery was made openly available after the mission ended.

These satellites have medium spatial resolution (tens to hundreds of meters), used for regional to global environmental monitoring.

| Satellite (Launch) | Spatial Resolution | Revisit Frequency | Operator | Data Access |
|---|---|---|---|---|
| **Sentinel-3A/3B (OLCI) (2016/2018)** | 300 m (optical multispectral) | ~1–2 days (with 2 satellites) | ESA/EUMETSAT (EU) | Open (Free) |
| **Terra & Aqua (MODIS) (1999/2002)** | 250 m (bands at best res) | Daily (Terra morning, Aqua afternoon) | NASA (USA) | Open (Free) |
| **Suomi NPP & NOAA-20 (VIIRS) (2011/2017)** | 375 m (visible/IR) | Daily (morning & afternoon orbits) | NOAA/NASA (USA) | Open (Free) |
| **Landsat 8 & 9 (Thermal)** | 100 m thermal IR | 8 days (global, combined) | NASA/USGS (USA) | Open (Free) |
| **PROBA-V (2013) – ◆Reduced ops** | 100 m (VNIR), 300 m (SWIR) | (Global 2-day until 2020; partial thereafter) | ESA/BELSPO (EU) | Open (Free) |
| **EnMAP (2022)** | 30 m (hyperspectral) | ~4 days (pointable) | DLR (Germany) | Open (Free) |
| **PRISMA (2019)** | 5 m pan; 30 m hyperspectral | ~7 days (pointable) | ASI (Italy) | Open (Free) |
| **Himawari-8/9 (2014/2016)** | 500 m – 1 km (visible bands) | 10 min (continuous geostationary imaging) | JMA (Japan) | Open (Free) |

**Table 5 Medium Resolution (10–100+ m) Satellites**

[24-50]

Free data access for registered scientific users (open data policy with registration) [50][42]

# Satellites and data acquisition

In recent years, the amount of free satellite data has grown in both variety and frequency, making it possible to create flood maps worldwide at a low cost.[51]

### Landsat

The development of Earth observation from space can be clearly seen in the Landsat program. Starting with Landsat-1 in 1972, the program has advanced its technology while consistently monitoring land surfaces. This long-term record has become an important reference for studying changes in Earth's land environment caused by both natural processes and human activities.[52]

Landsat 8 carries two key instruments, the Operational Land Imager (OLI) and the Thermal Infrared Sensor (TIRS), which together provide seasonal global land coverage with spatial resolutions of 30 meters (visible, NIR, SWIR), 100 meters (thermal), and 15 meters (panchromatic). Building on this, Landsat 9 was launched with upgraded counterparts, OLI-2 and TIRS-2, that use advanced technology to capture the highest quality data in 11 spectral bands, while ensuring full compatibility with previous Landsat records. Operating

in a near-polar orbit, Landsat 9 contributes over 700 new Earth scenes daily and, when combined with Landsat 8, enables repeat imaging of almost the entire globe every eight days. All collected data are archived and freely distributed by the USGS Earth Resources Observation and Science (EROS) Center, ensuring continuity of one of the most valuable long-term Earth observation records.[53], [54]

**Skysat**

SkySat, managed by Planet, is a high-resolution constellation of 15 satellites capable of revisiting any location on Earth up to ten times per day, with a daily imaging capacity of around 4,000 km². It enables tasking services, allowing users to define the time and place of image acquisition. The satellites generate orthorectified panchromatic and four-band imagery with a spatial resolution of 50 centimeters per pixel.[55]

| Band | Name | Wavelength |
|---|---|---|
| 1 | Blue | 450 - 515 nm |
| 2 | Green | 515 - 595 nm |
| 3 | Red | 605 - 695 nm |
| 4 | Near IR | 740 - 900 nm |
| NA | Panchromatic | 450 - 900 nm |

**Figure 8 Different bands of SkySat**

**Sentinel2**

Sentinel-2 is equipped with an optical payload that includes visible, near-infrared (NIR), and shortwave-infrared (SWIR) sensors, covering 13 spectral bands with spatial resolutions of 10, 20, and 60 meters across a 290 km swath. However, as an optical mission, its ability to monitor floods is limited to daytime and clear-sky conditions, since solar radiation in the visible range cannot penetrate cloud cover[56]

| Band | Name | Central Wavelength |
|---|---|---|
| B01 | aerosol | 443 nm |
| B02 | (blue) | 490nm |
| B03 | (green) | 560nm |
| B04 | (red) | 665nm |
| B05 | (red edge) | 705nm |
| B06 | | 740nm |
| B07 | | 783nm |
| B08 | (NIR) | 842nm |

| | | |
|---|---|---|
| B8A | | 865nm |
| B09 | | 945nm |
| B10 | | 1375nm |
| B11 | (SWIR 1) | 1610nm |
| B12 | (SWIR 2) | 2190nm |

**Figure 9 Sentinel-2 Bands**[57]

## Description of Copernicus Emergency management service (CEMS)

The European Copernicus program uses satellite sensors to support civil protection services through its Emergency Management Service (EMS). This service provides rapid damage assessment maps for natural or human-made disasters and operates 24/7. Requests for activation are approved by the European Commission via the Emergency Response and Coordination Centre (ERCC) at DG ECHO (Directorate-General for European Civil Protection and Humanitarian Aid Operations), and the full process, from activation to final map delivery, is managed through this service. [58]

**The EMS has two main parts:**

1. Mapping: including rapid mapping and risk/recovery mapping, which deliver digital and vector-based maps from satellite images to help emergency managers make informed decisions.

2. Early warning: mainly through the European Flood Awareness System (EFAS), which helps national and local authorities prepare before major flood events.

Since 2021, a global near-real-time flood monitoring system (GFM) has been added to the Global Flood Awareness System (GloFAS). This system processes all Sentinel-1 images using three advanced flood mapping algorithms (HASARD, ALGORITHM2, and ALGORITHM3) and combines their outputs to produce fast, reliable, and high-quality flood maps.[58]

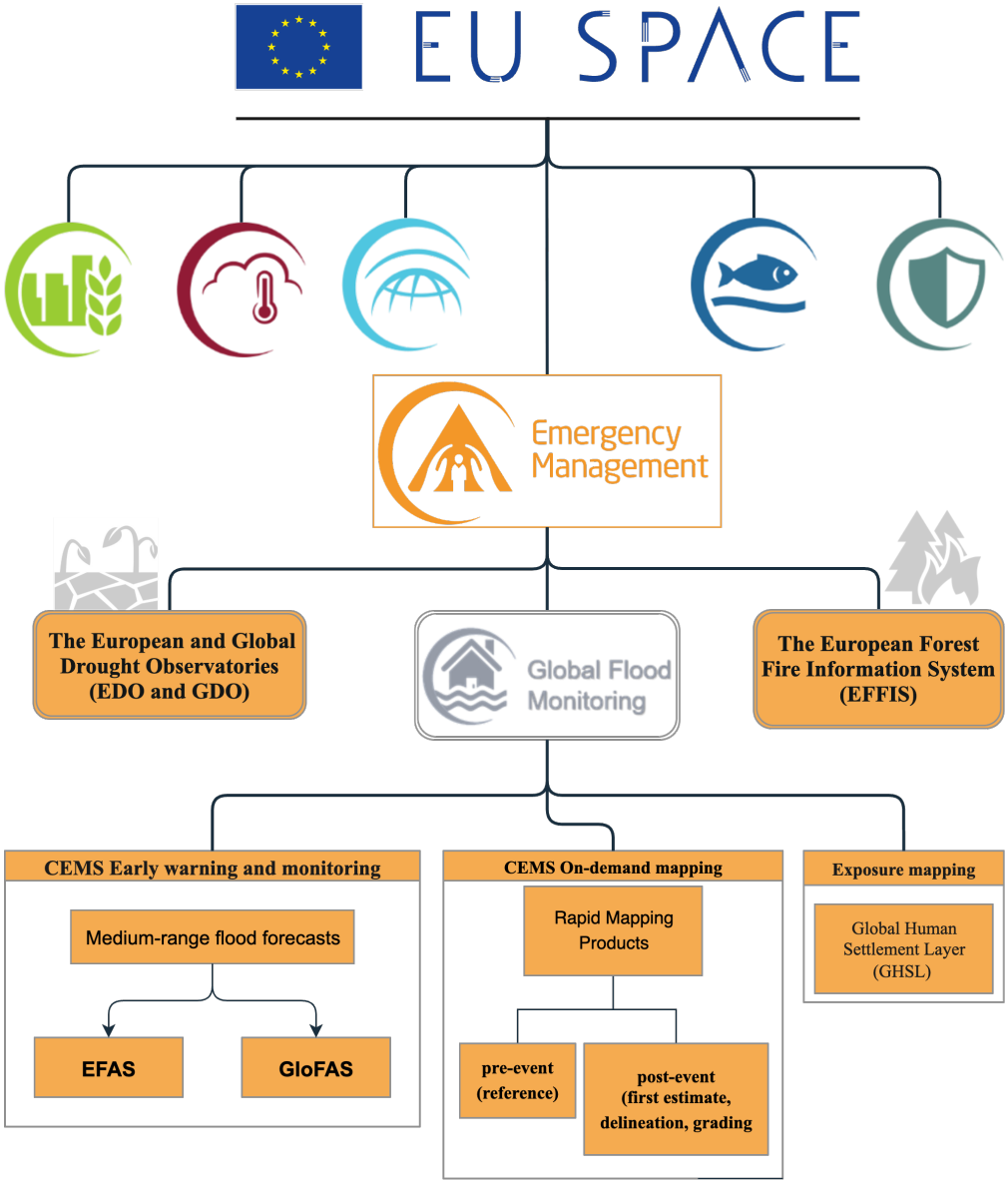


Figure 10 organization of EMS

# Rapid mapping and risk and recovery mapping

### delivered Products

Each Copernicus product is delivered in two formats: a ready-to-print map and a vector package that includes geographic datasets. These products follow a strict naming system

to keep them consistent. The quality of the input data affects the outcome. if the data quality is only medium, then a “partial release” is issued. Both the service provider and the European Commission’s Joint Research Centre (JRC) check the quality of every product, and if mistakes are detected, corrected versions are produced and released.[59]

Delivered maps are one of the main outputs of the Copernicus Emergency Management Service (CEMS) and other disaster response systems, providing essential geospatial information before, during, and after flood events. The two most common types are delineation maps and grading maps.

• Delineation maps show the exact extent of flooding, usually based on satellite data such as Sentinel-1 or Sentinel-2. They highlight the areas covered by water and are produced quickly, often within hours, to support emergency operations by indicating which regions, infrastructures, and settlements are inundated.

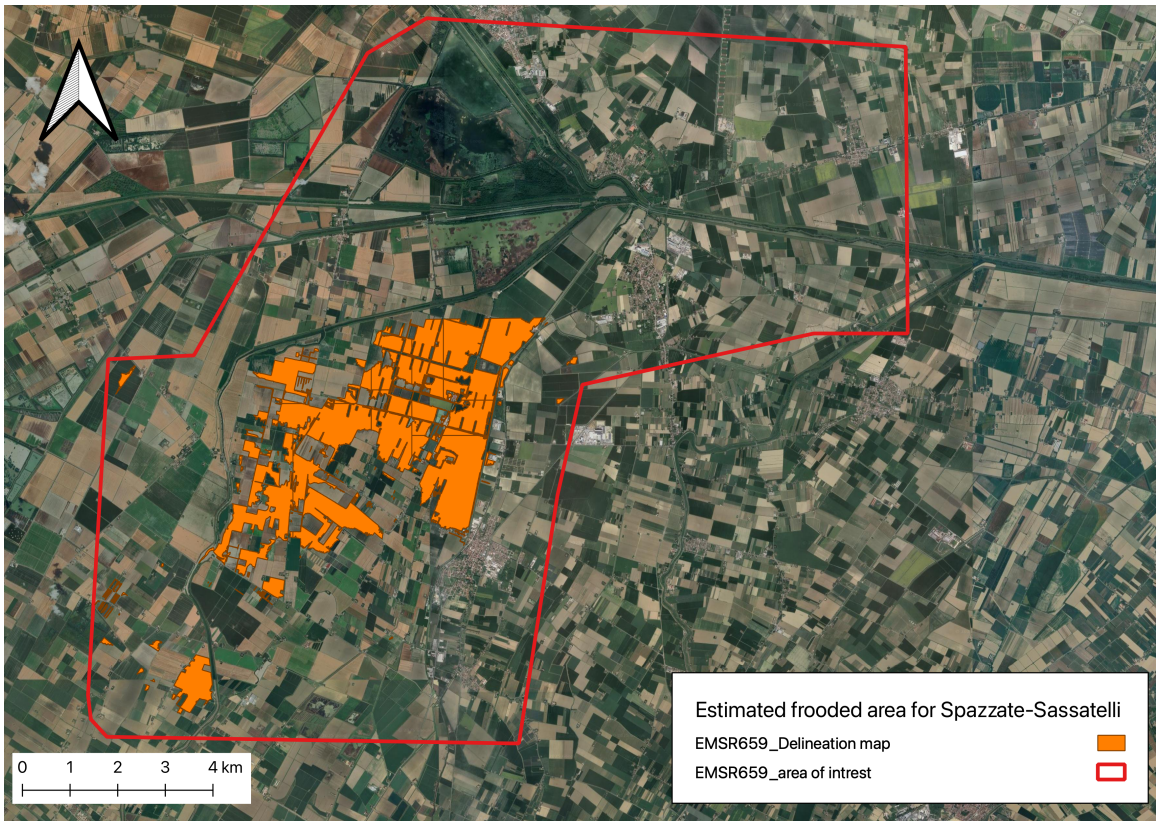


Figure 11 Delineation map version 1

• Grading maps go further by assessing the level of damage across different sectors, including housing, transport, public services, and land use. They categorize the damage (e.g., destroyed, damaged, or possibly damaged) and are especially useful for recovery planning, resource allocation, and insurance purposes[60],[61]

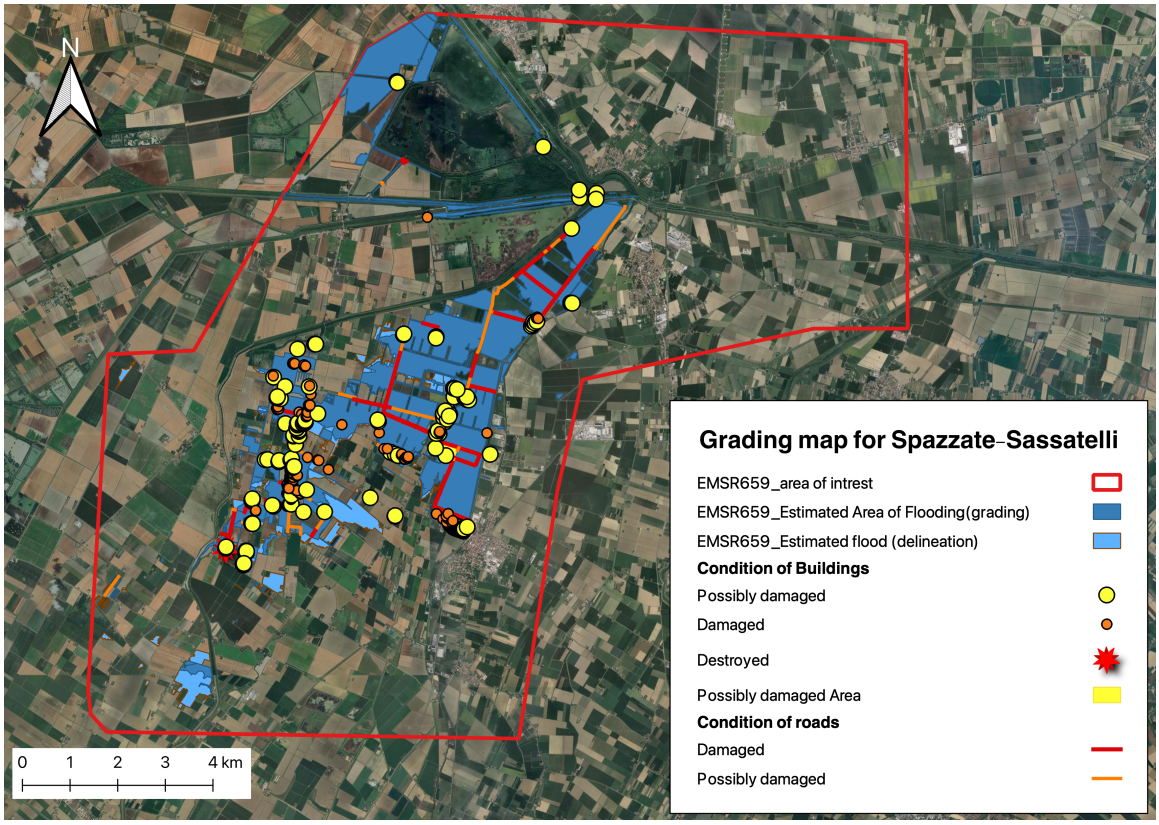


Figure 12 Grading map last released report

## Timeline for emergency response

In flood mapping and specifically critical situations, time is a key factor. “For the 14 activations related to an EFAS pre-tasking request, the first crisis information provided was delivered on average 16:05 h after the activation start. Without pre-tasking, the delivery time for the first product was on average 28:47 h after the activation start.”[62]

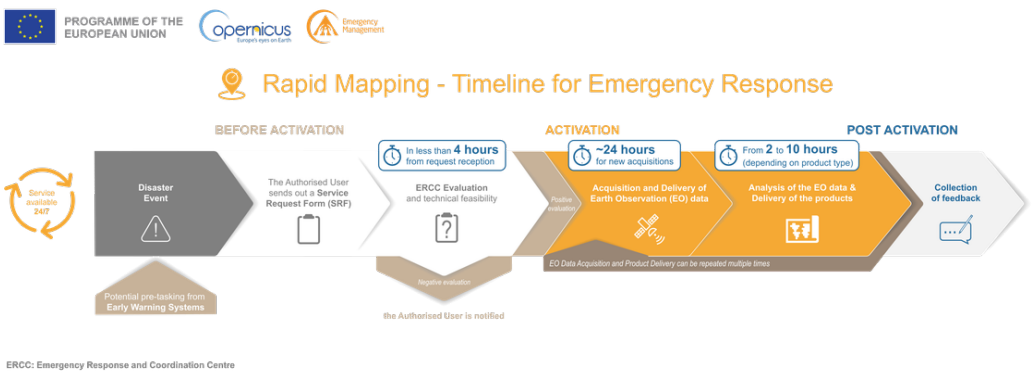


Figure 13Timeline for EMS[81]

## Review of EO-based flood extent and depth mapping

Estimation of flood depth is much harder and equally important as flood extent estimation to address the risks and emergency responses[63]. Teng J et all.(2022) assessed three simple models to estimate depth of flood water by varied DEM inputs. In this research showed that FwDET (Floodwater Depth Estimation Tool) was the best in performance, HAND (Height Above Nearest Drainage) was suitable for users who have access to flood extent and TVD( TengVaze Dutta) was very good at deep waters.[63] FwDET determines water depth by subtracting the local floodwater elevation (measured above mean sea level) from the topographic elevation at each grid cell within the flooded area. This flooded area is supplied to FwDET as a GIS polygon layer or optionally as a raster when using FwDET-GEE, allowing flexibility regardless of how the flood extent was originally derived. Both the elevation of the terrain and the floodwater are obtained from a Digital Elevation Model (DEM). Although any DEM can be used, its spatial and vertical resolution significantly influences the accuracy of the depth estimates.[64]

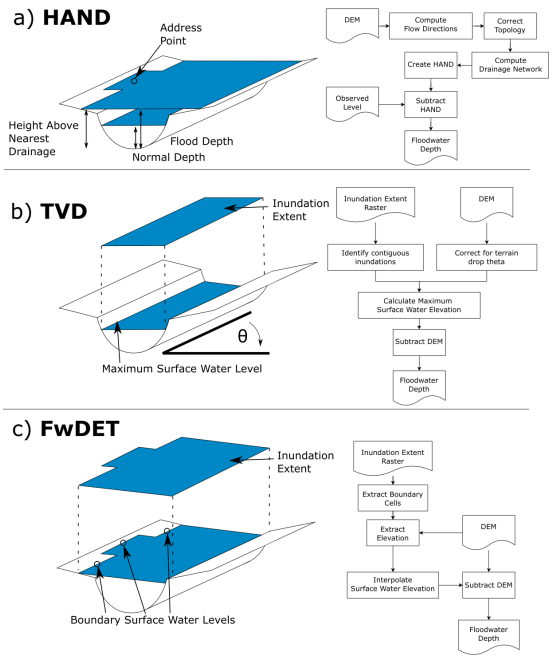


Figure 14 methods of estimation of flood depth [63]

HAND estimates flood depth at specific locations by combining observed water levels with a Digital Elevation Model (DEM). TVD determines the maximum surface water level in flooded regions

using a flood extent raster and a DEM adjusted for terrain slope. FwDET calculates flood depth by using a flood extent raster and a DEM, estimating surface water levels by interpolating from the boundary of the inundated area.[63]

Another method called FLEXTH is used to estimate flood depth and enhance flood mapping by utilizing inundation maps, easily accessible Digital Terrain Models (DTMs), and open-source software. The approach is largely automated, requiring minimal user input, and can process very large regions efficiently[65].

# K-means Clustering

Clustering is a common method used in data science to group similar data points together and separate them from those that are different. There are four main types of clustering methods:

1. Connectivity-based clustering: groups data points based on how close they are to each other.
2. Centroid-based clustering: represents each cluster by a central point (called a centroid).
3. Distribution-based clustering: groups data that follows the same statistical pattern.
4. Density-based clustering: forms clusters where data points are densely packed, while points in sparse areas are treated as noise.

To group data effectively, clustering methods need a way to measure how similar or different data points are. One of the most popular centroid-based methods is K-means clustering. It is an unsupervised algorithm, meaning it does not require labelled data. K-means divides a dataset into a chosen number of groups (K) based on the similarity between data points.

The algorithm works by finding the center (centroid) of each cluster and assigning every data point to the nearest centroid. It then updates the centroids repeatedly until the positions stop changing. The goal is to minimize the distance between data points and their cluster centers. This is represented by the following equation:

$$L_{km} = \sum_{k=1}^{k} \sum_{i \in G_k} \|x_i - b_k\|^2$$

where K is the number of clusters, $G_k$is the group of data points in cluster k, and $b_k$is the centroid of that cluster. K-means is a fast and simple algorithm that works well with large datasets and produces good results in many applications. However, it has one main limitation it is sensitive to the number of clusters chosen. If K is not selected properly, the results may not represent the data accurately.[66]

# Accuracy assessment

Accuracy assessment is a fundamental process in evaluating the reliability and performance of classification results derived from remote sensing or spatial analysis. It measures the degree of agreement between a model and the reference, or "ground truth data" [67].

Among the available various metrics, Precision, Recall, and the F1-score are commonly employed because they provide complementary insights into the classification performance. These metrics are derived from the confusion matrix, which summarizes the relationship between predicted and observed classes in terms of true positives (TP), false positives (FP), false negatives (FN), and true negatives (TN)[68].

**Precision**

measures the proportion of correctly predicted flooded layer relative to all pixels identified as flood by the ground truth data, which is CEMS, indicating how many pixels of the detected floods are truly correct. It is defined as:

$$precision = \frac{TP}{TP + FP}$$

High precision implies that most of the areas detected as flooded correspond to actual floods, reflecting a low rate of false alarms[69]

**Recall**

also known as sensitivity or true positive rate, measures the proportion of actual flooded areas that were correctly identified by the algorithm. It is calculated as:

$$Recall = \frac{TP}{TP + FN}$$

A higher recall indicates that the model effectively detects most of the real flood extents, even if it occasionally misclassifies non-flooded regions as flooded[70]

**F1-score**

combines both precision and recall into a single indicator by calculating their harmonic mean:

$$F1 - \ score = \frac{2 \times precision \times recall}{precision + recall}$$

This metric provides a balanced measure between omission errors (missed floods) and commission errors (false detections) and is particularly useful when the dataset is imbalanced, meaning that flooded and non-flooded areas are not equally represented [71]

# Methodology

The main aim of the study is to propose an efficient and user-friendly method to achieve flooded area raster layer in a logical time for two different sources of data, Sentinel 2 and Skysat. Furthermore, comparison of open-source data and commercial data by implementing a machine learning method and finally data trustworthy by validation methods. For this thesis, a set of computer codes was developed to detect and map floods using satellite images. The code framework was designed in a modular way, meaning each part of the code has a clear role, and all parts work together to produce the final flood extent. It should be mentioned that an unsupervised machine learning method called k-means clustering which is part of partitional (or centroid-based) clustering was used to separate water from non-water areas.

**Overall workflow**

Two different ways of getting floodmap from the Sentinel-2 and Skysat data has been implemented. To achieve the results, due to the lighter volume of data for sentinel-2, a cloud based Jupiter notebook environment that is provided by google has been used which is termed Google colab. Advantage of Google colab is free access to computing resources, including GPUs and TPUs; nevertheless, In the free version of Colab that is free of charge there is very limited access to GPUs. Usage limits are much lower than there are in paid versions of Colab. With paid versions of Colab it is possible to upgrade to powerful premium GPUs subject to availability and your compute unit balance. It should be mentioned that the algorithm for sentinel data works very well with the free version of Colab.

In the second attempt, to achieve the inundated layer, Skaysat data has been used. In this data because of more volume of data, Google Colab was not proper, specifically in the desired raster file which should be uploaded on the local files of Colab. So, it increase the time of process besides the limitation of computing in this environment. In this reason, data processing has been done in the local computer with Visual Studio code editor. In both cases methods are similar but some codes are different in each. The general workflow is in this order:

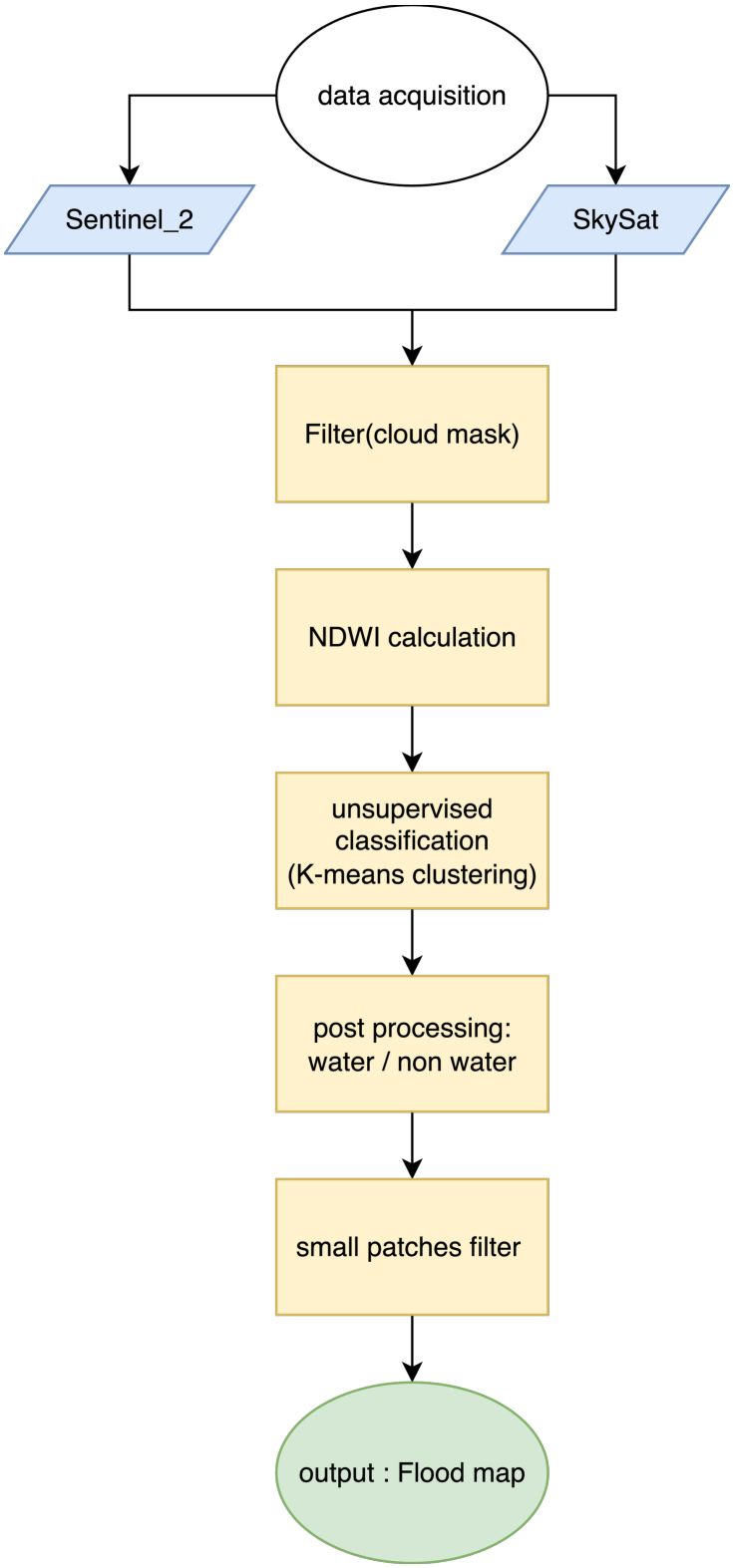


Figure 15 workflow of the process

All the executed codes are available in represented repository, included NDWI_open-source-data and Local-GeoTIFF-skysat, in the GitHub website[72].

# Data and Tools

### Datasets

In this thesis four datasets have been utilized. The open source data , specifically Sentinel-2,is taken from European satellite earth observation organization which is termed Copernicus data space Ecosystem and for commercial ultra-high images SkySat images from company named Planet, Copernicus emergency management service reports, which provide delineation and grading maps which uses two different SAR datasets ,PAZ & Cosmo, in order to have a robust ground data for water detection.

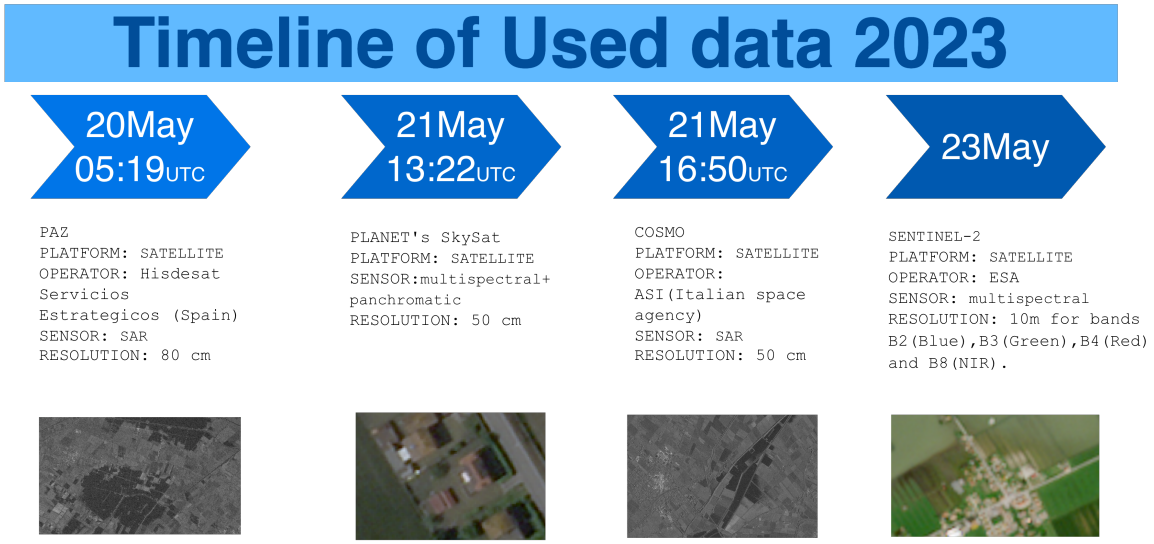


Figure 16 timeline of data [74][75][76][77][83]

### Software and Tools

Data processing and analysis were carried out using a combination of open-source data, commercial data and codes. QGIS (version 3.28.3-Firenze) was used for spatial visualization. To handle large geospatial datasets and perform flood mapping analyses, Python codes were written and implemented using two platforms: Visual Studio Code (VS Code), which was primarily used for local data processing and debugging, and Google Colab, which was utilized for cloud-based execution due to its computational efficiency and integrated libraries. The scripts incorporated packages such as GDAL, Rasterio, Pandas, and Google earth engine (GEE) to preprocess satellite imagery, calculate water index, and generate classified flood maps.

**Data limitations**

Although open-source data like CDSE (Copernicus Data Space Ecosystem) offer vast amount of data, but the scarcity of exact time and date is felt in this study. Mostly it is hard to find the exact time of happened event to monitor the event. Besides that, resolution of free data is not comparable to commercial data. Another limitation is availability of high or ultra-high resolution data. For acquiring the resolution, bellow the 3m approximately, the good amount of money should be paid to access these data.

# Data processing

**Sentinel-2 pipeline (Google Colab)**

In this part, the code uses Google Earth Engine (GEE) platform to import Sentinel-2 satellite images with requested date and other details, together with Google Colaboratory (Colab) as the working environment. Colab is a hosted Jupyter Notebook service that requires no setup and provides free access to computing resources, including GPUs and TPUs, which makes it convenient for running the workflow online without the need for local installations of packages. The code automatically downloads images for the study area, removes cloud-covered pixels, and calculates the Normalized Difference Water Index (NDWI) to highlight water. For sentinel-2 there are two main bands should be considered for extraction of water layer. Band 3 for Green and band 8 for near IR. so the formula for Sentinel 2 is in this order:

$$NDWI = \frac{B3 - B8}{B3 + B8}$$

A k-means clustering method is then used to separate flooded areas from non-flooded ones. Permanent water bodies are removed to keep only newly flooded areas, and small noise patches are filtered out. The images are then mosaicked by date and labelled, making it possible to track flooding across time. With this method it's possible to have a flood map less than 1 minute. The main code and the modular helpers are in this order: In the main code there is a close contact with google earth engine. In this part, all the main features such as details of area of interest, flood event data, cloud threshold which sets the maximum acceptable cloud coverage and lags for time range (days) after event are taken to execute the order. modular helpers are in this order and are imported in the main code:

| Module | Purpose | Key functions | Inputs | Outputs |
|---|---|---|---|---|
| Upload.py | -Load Sentinel-2 L2A image collection for a given area and date range.<br>- Generate a mask of permanent water bodies | -ee.ImageCollection<br>-filter<br>-water_history | -Image from<br>-satellite | -s2_collection<br>get_permanent_water |
| date_utilize.py | -Compute post-flood and reference date ranges from a flood event date. | -Parse<br>-format | -event_date_str<br>-post_lag<br>-days_before_start<br>-days_before_end | get_date_ranges |
| filter.py | -Remove Small Flood Areas | -process_image<br>-mask_clouds | -mask_collection<br>-roi<br>-min_area | -mask_clouds,<br>remove_small_area |
| Threshold.py | -Classification on NDWI | -Clusterer<br>-Clustered<br>-flood_cluster<br>-flood_mask | -ndwi_img, aoi,<br>-n_clusters=2 | classify_kmeans |
| Mosaic.py | -Mosaic Sentinel-2 images by acquisition date using median.<br>-Keeps only mosaics that fully cover the AOI. | -add_date<br>-mosaic_on_date | -collection<br>- roi | -mosaic_s2 |

Table 6 modules with their function

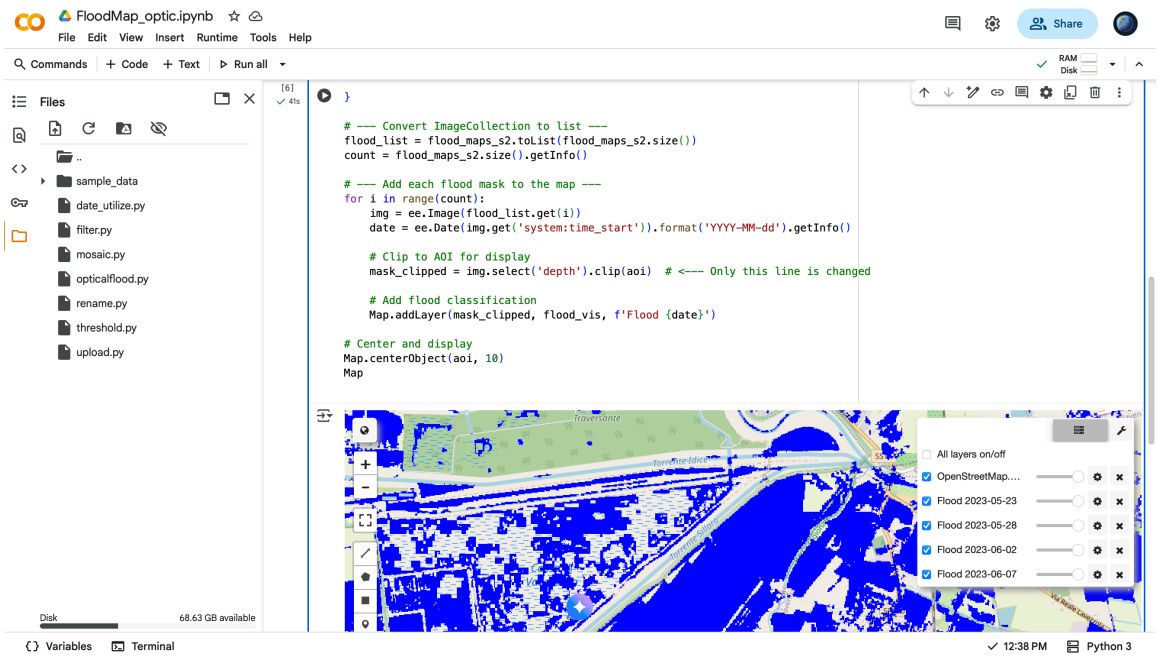


Figure 17 executed codes in Colab and Flood map

The workflow of open- source data code is illustrated in the next page:

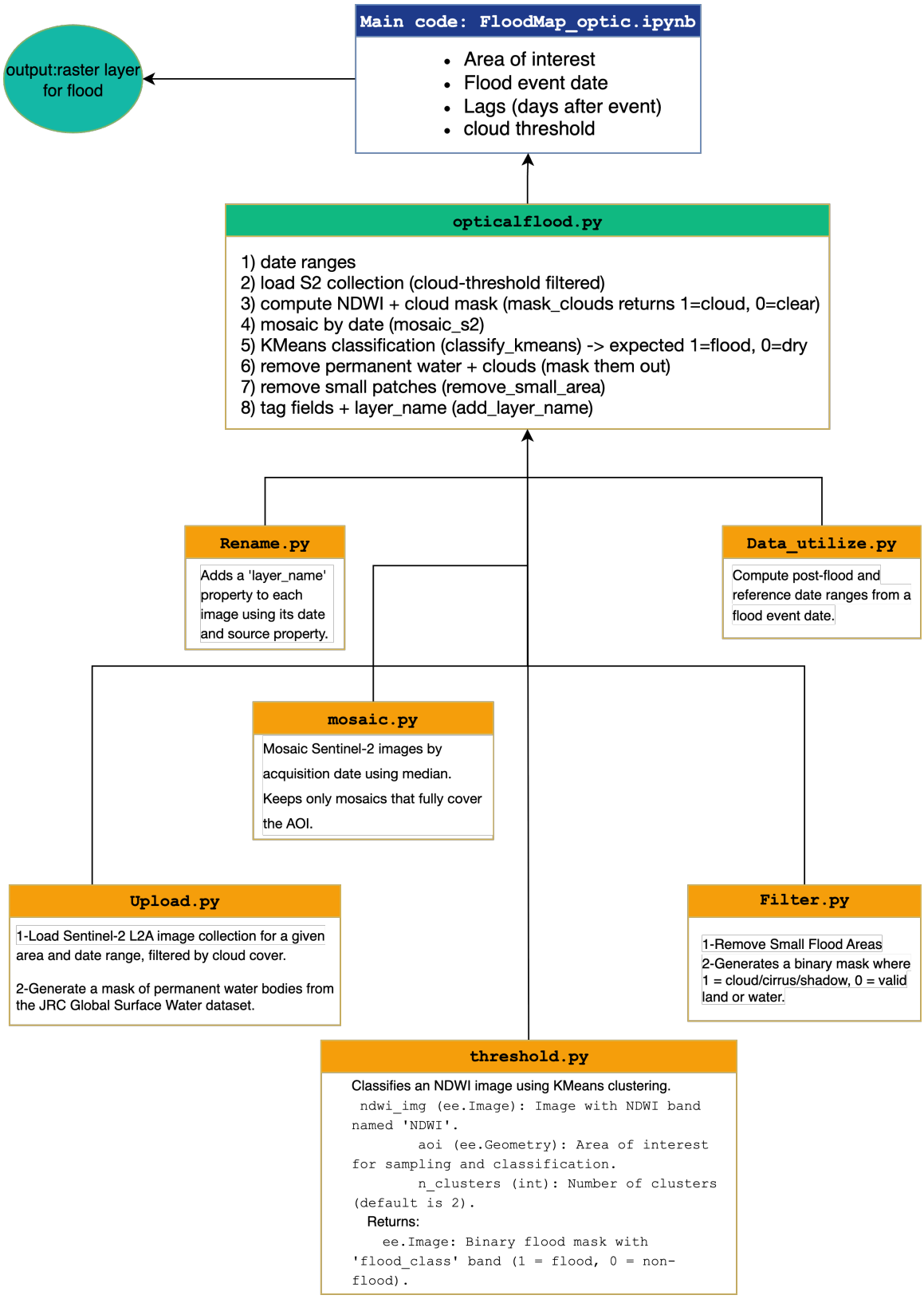


Figure 18 Sentinel-2 workflow

**SkySat pipeline (Local processing)**

In the SkySat image we have higher data resolution besides 5 different spectral Bands. To calculate the NDWI for our data bands 2 and 4 as Green and NIR should be considered.

$$NDWI = \frac{B2 - B4}{B2 + B4}$$

This prompt has done with the codes besides using several Python Standard Libraries and Numerical Packages:

| Package | Purpose |
|---|---|
| os | File and directory operations, environment variables, paths |
| json | Read/write JSON data for configs or metadata |
| warnings | Manage warning messages (e.g. suppress GDAL/rasterio warnings). |
| contextlib | Provides contextmanager decorator for creating custom with ... blocks (used to manage GDAL environment). |

**Numerical Packages**

| | |
|---|---|
| NumPy | Core array & matrix math; numerical operations, masking, statistics. |
| SciPy (ndimage) | Morphological image processing (e.g., binary_opening, binary_fill_holes, label), smoothing, filtering, connected components. |

**Geospatial / Remote Sensing Packages**

| Package | Purpose |
|---|---|
| rasterio | Read, write, and manage raster (GeoTIFF) data. Interface to GDAL. Handles CRS, transform, metadata. |
| rasterio.enums | Provides resampling methods (nearest, bilinear, cubic) for reprojection/resampling. |
| rasterio.warp | Function to reproject raster between different CRS or align to a target grid. |

**Machine Learning & image processing packages:**

| | |
|---|---|
| scikit-learn | Unsupervised clustering (e.g., K-means for separating water/non-water classes). |
| Pillow (PIL) | Handles non-georeferenced image operations like saving previews (PNG/JPEG), visualization, array-to-image conversion. |

Table 7 used packages in the helper module

The workflow of Skysat code is depicted in the next page:

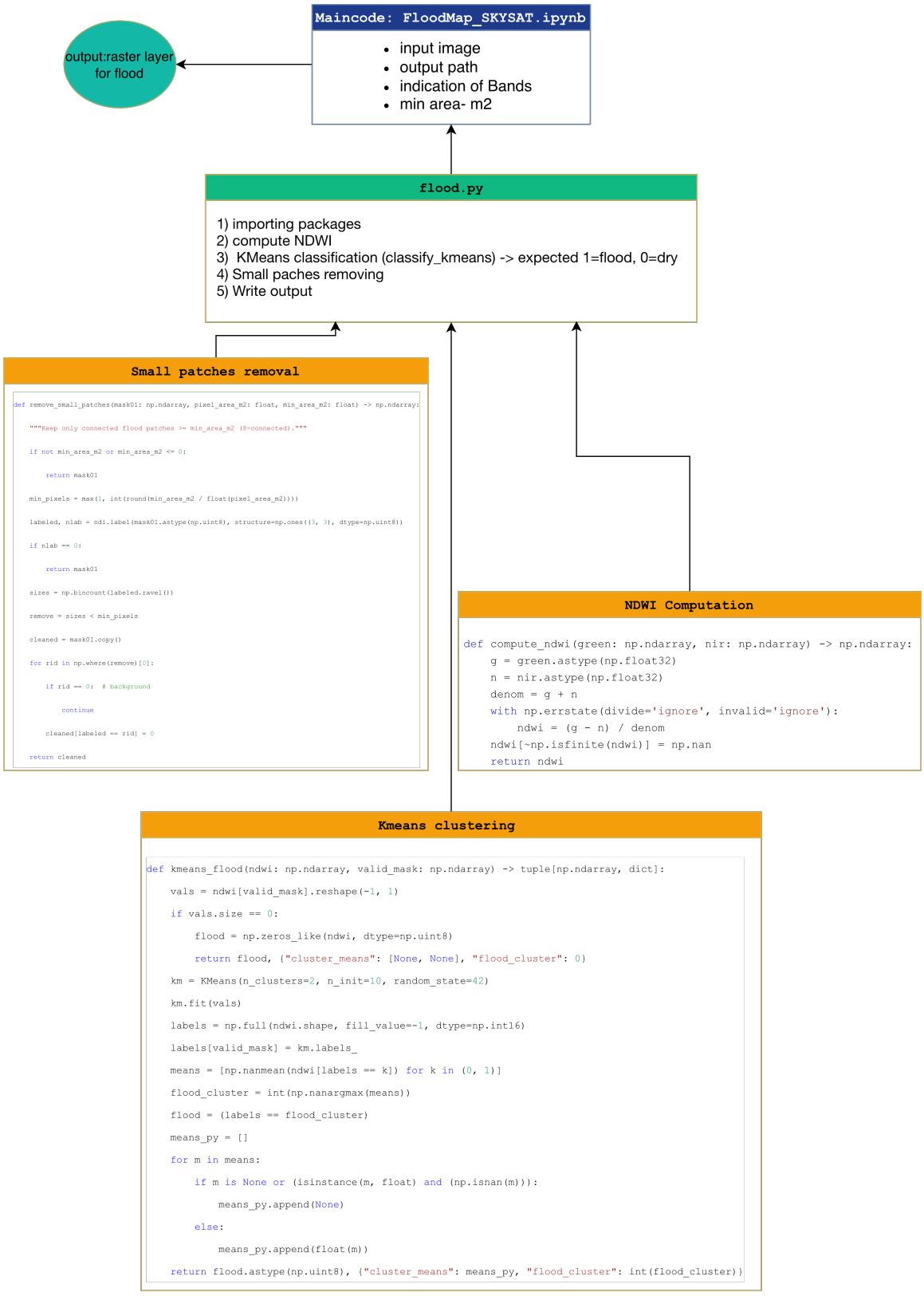


Figure 19 SkySat workflow

While Google Colaboratory and Earth Engine were used for cloud-based processing, Visual Studio Code (VS Code) Version: 1.104.1 served as the primary local development environment for building and running the Python modules for this part of the study. It works on very high-resolution satellite images stored locally on the computer. By the code, it reads the Green and Near-Infrared (NIR) bands, calculates NDWI, and classifies water by clustering, also it can clean the results by removing very small patches.

This approach is especially useful for small study areas where detailed, high-resolution images are needed. The reason which these codes are not executed on Google Colab is the limitation of access to computing resources in this service, so for huge data using more powerful processor or buying the full access to Google Colab is a must. The processing takes, based on provided data, generally 4 or 6 minutes until the final result is saved on output folder in the local computer. This test was done on a MacBook pro with a M1 processor and 16 GB of RAM. The time can change depending on the computer's hardware and the size of the input file. All analyses were implemented in Python v3.11.13 using a modular architecture.

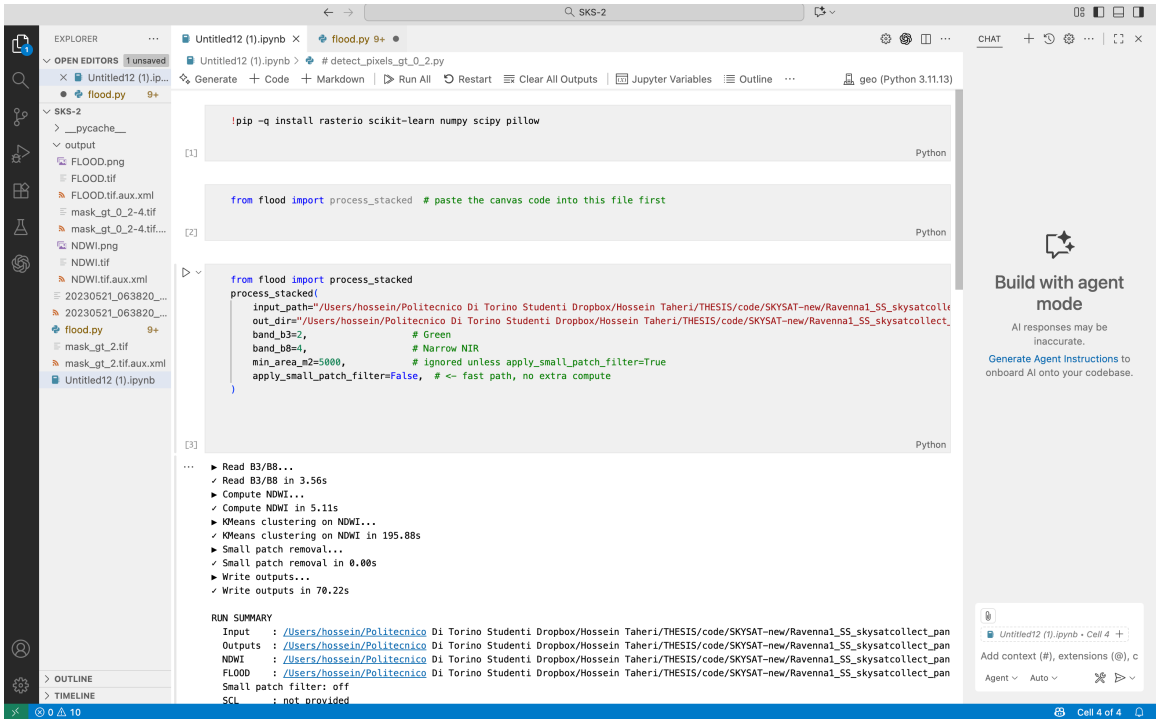


Figure 20 atmosphere of VScode and the executed code

# Results

This chapter presents the results of applying the developed flood mapping framework to Sentinel-2 and SkySat imagery. The findings are organized into three parts: (1) flood extent mapping, (2) processing times, and (3) accuracy comparisons. Together, these results demonstrate the performance and applicability of the proposed methodology.

## Flood Extent Maps

The framework successfully produced flood maps from both Sentinel-2 and SkySat datasets.

## Sentinel-2 outputs

The Sentinel-2 pipeline generated regional flood extent maps at 10 m spatial resolution. These maps provided a clear overview of the inundated areas, making it possible to rapidly assess the flood event across the region in two different dates 23 and 28 of may2023, however due to the reason ground truth data , Cosmo with SAR data,  is taken on 21 of May, it is decided to choose the nearest time which is 23 of May.

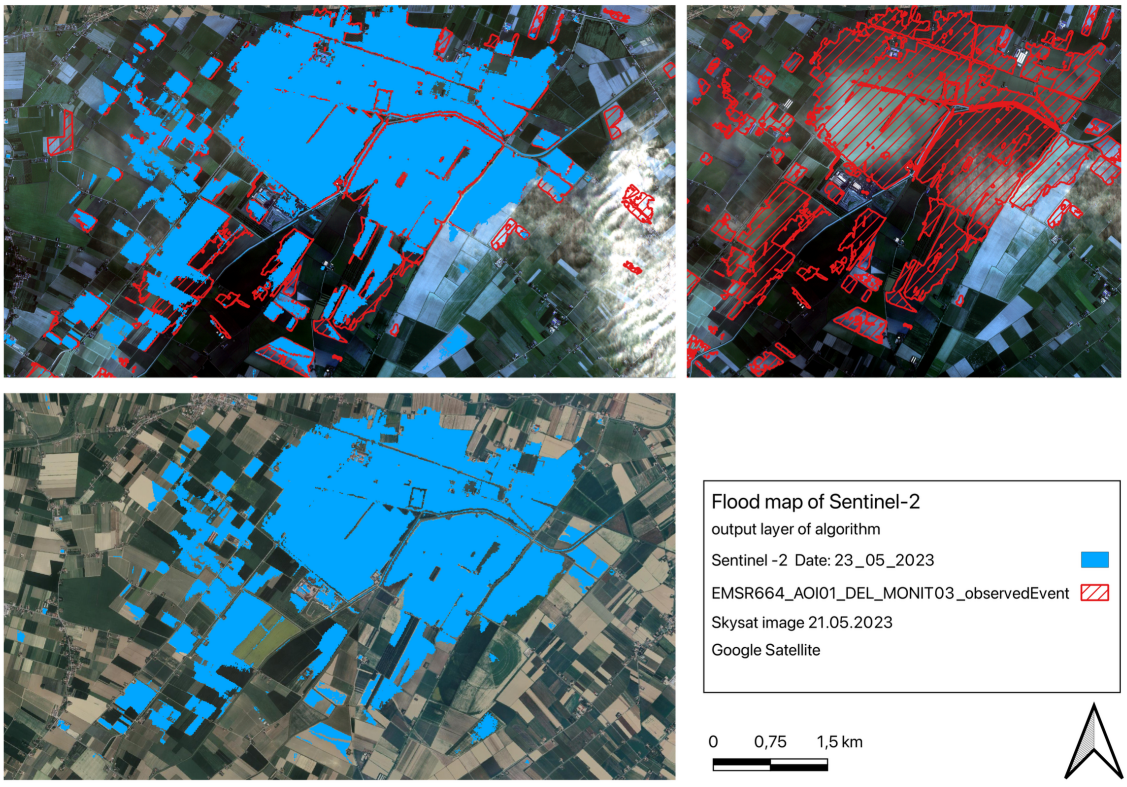


Figure 21 comparison EMS report and acquired results

# SkySat outputs

The SkySat pipeline produces much higher resolution flood maps (sub-meter level). These results were particularly valuable for detecting smaller water bodies, narrow inundation lines, and floodwater in urban environments like pavements, streets and roads. Compared to Sentinel-2, SkySat outputs revealed more detailed boundaries of the flooded area and reduced errors in complex landscapes.

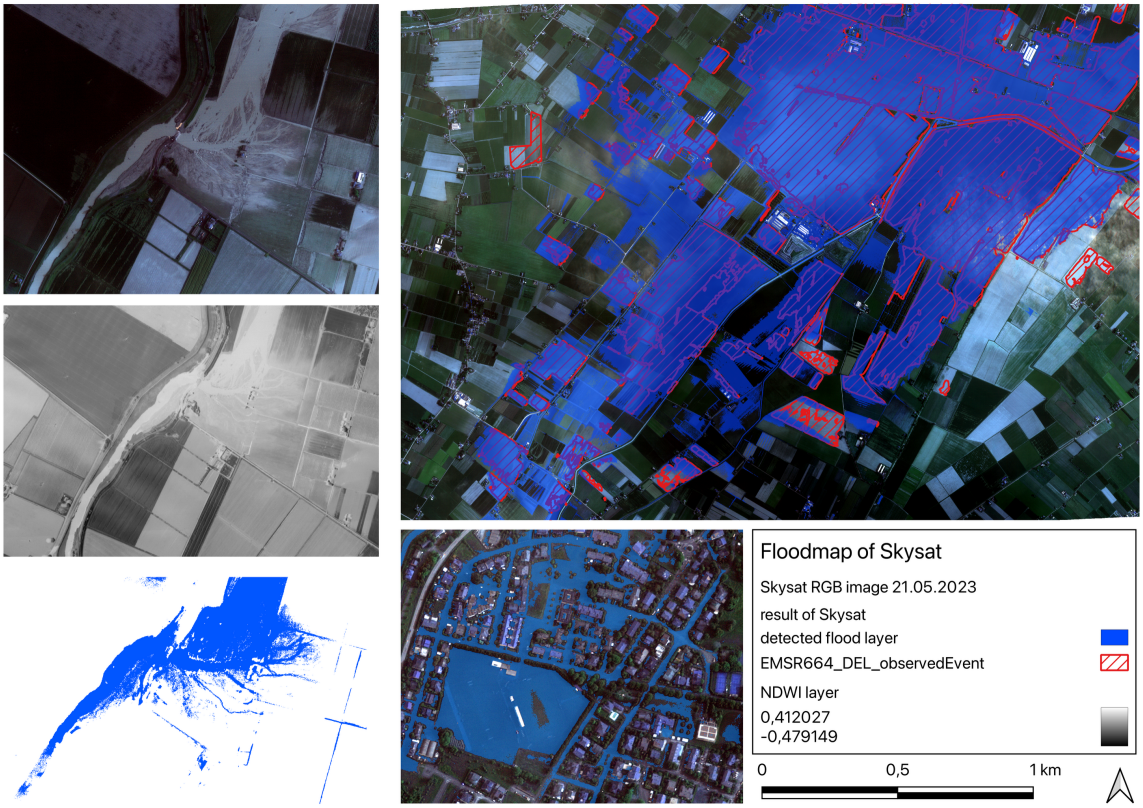


Figure 22 result of high-resolution data

# Processing Time

The time performance of the two pipelines was also evaluated.

## •Sentinel-2 (Google Colab):

Processing in Colab was almost fast, with flood maps generated in less than one minute. This is achieved thanks to the cloud-based infrastructure, which eliminates the need for a local computer.

## •SkySat (Local Processing):

The SkySat pipeline was executed on a MacBook with an M1 processor and 16 GB of RAM. The time required to process a single tif file with the size of about 1.5 GB and generate the final flood mask was approximately 4 to 5 minutes, nevertheless, it is totally related to the volume of input data and configurations of used computer.

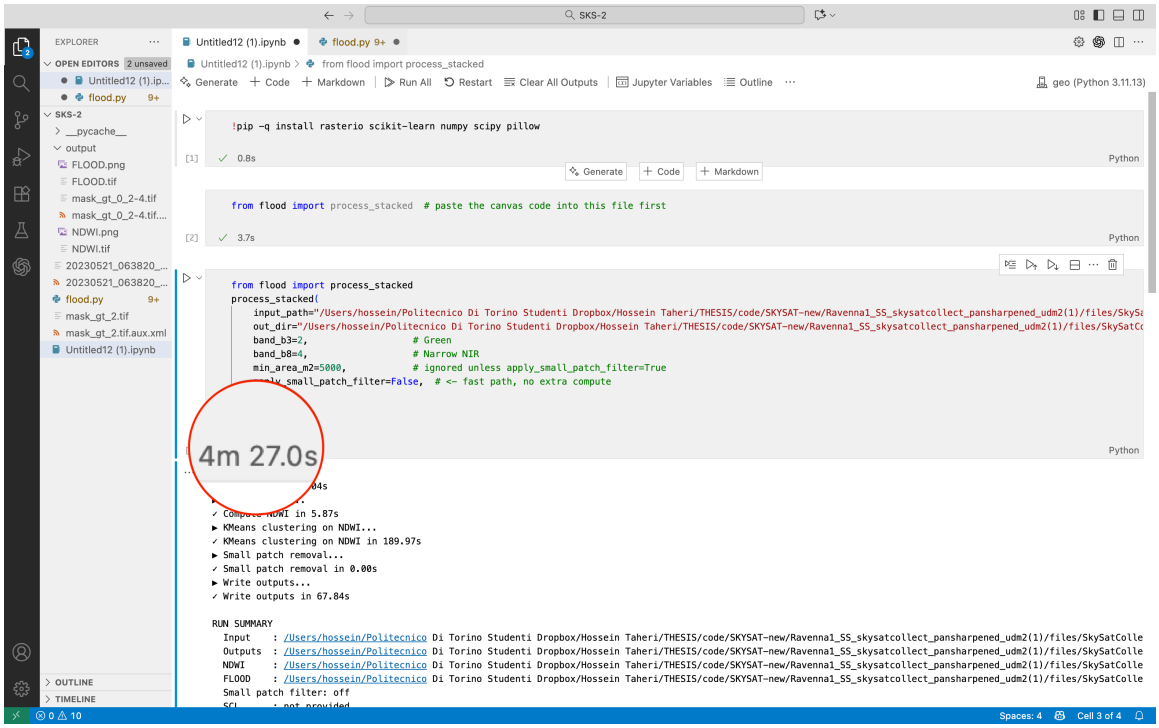


Figure 23 time of code execution

# Accuracy assessment

In this matter, three assessment such as precision and recall and F1-Score has been done. It should be mentioned that Copernicus emergency management service results have been used as ground truth data. The ground truth data is originally SAR data from COSMO and PAZ satellites, so the ground truth data is highly trustworthy.

## •Sentinel-2 accuracy:

At the regional scale, the results from Sentinel-2 achieved good agreement with reference data. However, there are some small areas which is not detected in my results compare to EMS report.

| | |
|---|---|
| Precision | 0.8462 (84.6%) |
| Recall | 0.7372 (73.7%) |
| F1-score | 0.7879 (78.8%) |

Table 8 assessment for Sentinel-2 workflow

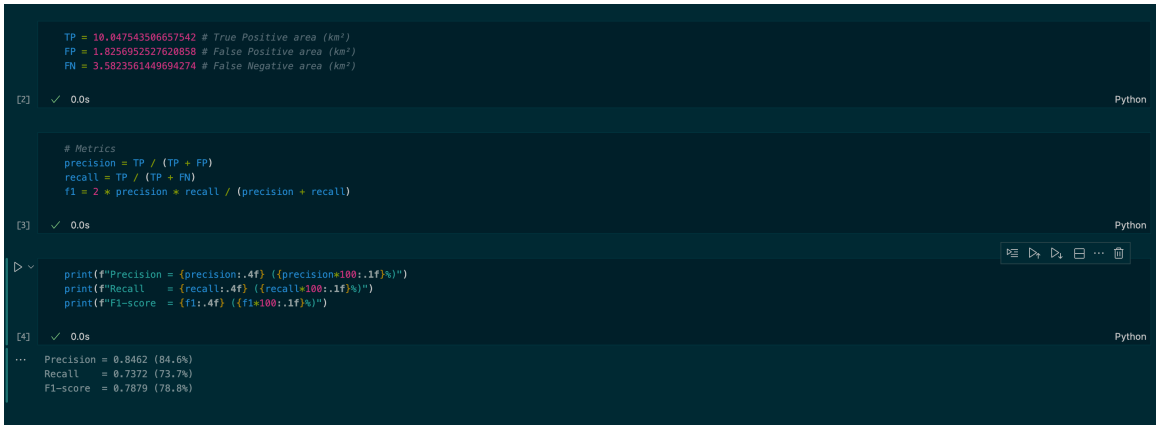


Figure 24 results in Vs code

## •SkySat accuracy:

SkySat results provided higher precision, particularly in urban zones and narrow floodplains. The high-resolution data allowed, in precision assessment, 7 out 10 pixels roughly detected correctly flood, while 3 out of 10 were false positive. This happens because of the area of interest and some parts which are included in ground truth data and excluded in Skysat result. Overall, it presents acceptable results.

| | |
|---|---|
| Precision | 0.7156 (71.6%) |
| Recall | 0.8976 (89.8%) |
| F1-score | 0.7963 (79.6%) |

Figure 25assessment for Skysat workflow

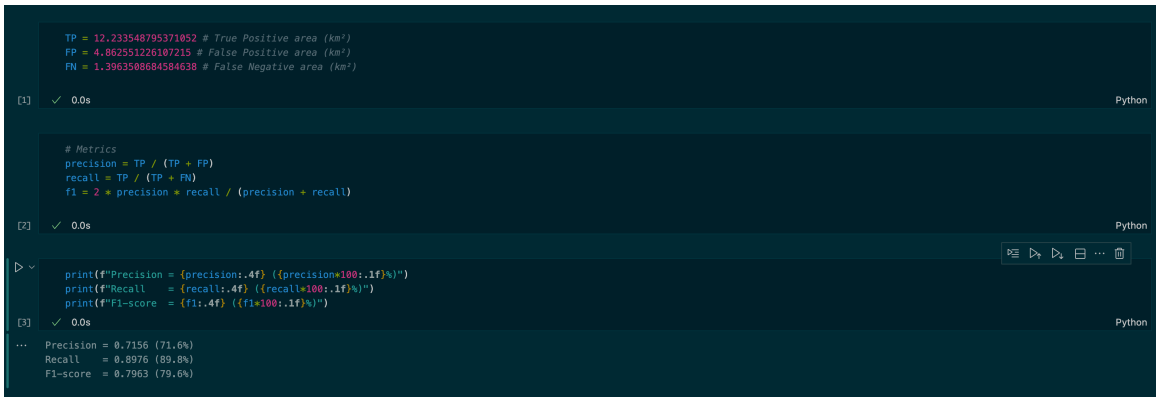


Figure 26 results in Vs code

# Summary of Findings

•The framework successfully generated flood maps for both Sentinel-2 and SkySat datasets.

•Sentinel-2 ensured fast, while SkySat provided fine-scale detail.

•Processing time was minimal in Earth Engine (<1 minute per scene) but longer in local processing (4-5 minutes per file on M1 MacBook, 16 GB RAM).

• The accuracy results show that both the Sentinel-2 and SkySat algorithms performed well in detecting flooded areas, but each has different strengths. The Sentinel-2 algorithm achieved higher precision (84.6%), meaning it was more accurate in identifying actual flooded pixels and made fewer false detections of non-flooded areas. However, its recall (73.7%) was lower, indicating that it missed some true flooded regions. In contrast, the SkySat algorithm had a lower precision (71.6%) but a higher recall (89.8%), meaning it detected most of the real flooded areas but also included more false positives. The F1-score, which balances precision and recall, was similar for both methods (78.8% for Sentinel-2 and 79.6% for SkySat). Overall, Sentinel-2 provides more reliable and cleaner flood detection, while SkySat is more sensitive and captures a larger extent of the flood, even if it slightly overestimates the flooded area.

# Conclusion

In this study two algorithms for open-source satellite data and commercial high-resolution imagery to produce flood maps has been created based on machine learning method K-means clustering and has been analyzed accuracy assessment for each. With a specific focus on the May 2023 flood event in the Spazzate-Sassatelli area of Emilia Romagna. The findings demonstrate that the developed Python-based workflow can generate flood maps in less than one minute for open-source data and about 4-6 minutes for commercial data depending on the volume of provided data. When compared with the official EMS report, the implemented approach proved to be highly efficient, offering timely outputs suitable for emergency applications. Furthermore, better illustration of inundated areas as a matter of details, like roads and streets for damage assessments and critical zones in danger with ultra-high resolution images from satellite.

In addition to the processing speed, Open-source data is more suitable for monitoring larger regions, while commercial ultra-high-resolution imagery provides detailed insights into critical zones, including streets and built environments, which are crucial for damage assessment and risk management.

The results show that the Sentinel-2 algorithm is more accurate but slightly misses some flooded areas, while the SkySat algorithm detects more flooded regions but includes more false positives. Overall, both perform similarly, with Sentinel-2 providing cleaner results and SkySat offering more details for flood detection. it should be mentioned that in both cases F1-score as was almost 80%.

Future work should integrate advances in Earth observation and machine learning to improve accuracy, reduce dependency on manual intervention, and enhance the reliability of real-time disaster mapping.

# References


[1] A. Domeneghetti, G. J.-P. Schumann, and A. Tarpanelli, "Preface: Remote Sensing for Flood Mapping and Monitoring of Flood Dynamics," *Remote Sens (Basel)*, vol. 11, no. 8, p. 943, Apr. 2019, doi: 10.3390/rs11080943.

[2] B. Bhattacharya, M. Mazzoleni, and R. Ugay, "Flood Inundation Mapping of the Sparsely Gauged Large-Scale Brahmaputra Basin Using Remote Sensing Products," *Remote Sens (Basel)*, vol. 11, no. 5, p. 501, Mar. 2019, doi: 10.3390/rs11050501.

[3] M. Valente *et al.*, "Health System Response to the 2023 Floods in Emilia-Romagna, Italy: A Field Report," *Prehosp Disaster Med*, vol. 38, no. 6, pp. 813–817, Dec. 2023, doi: 10.1017/S1049023X23006404.

[4] "https://rapidmapping.emergency.copernicus.eu/EMSR659/download."

[5] L. Warnecke, "NASA as a Catalyst: Use of Satellite Data in the States."

[6] T. J. Cova, "ch60," 1999.

[7] A. Kawasaki, M. L. Berman, and W. Guan, "The growing role of web-based geospatial technology in disaster response and support," *Disasters*, vol. 37, no. 2, pp. 201–221, Apr. 2013, doi: 10.1111/j.1467-7717.2012.01302.x.

[8] B. Tomaszewski, M. Judex, J. Szarzynski, C. Radestock, and L. Wirkus, "Geographic Information Systems for Disaster Response: A Review," Sep. 01, 2015, *Walter de Gruyter GmbH*. doi: 10.1515/jhsem-2014-0082.

[9] R. Sivanpillai, B. K. Jones, and R. M. Lamb, "Accessing satellite imagery for disaster response through the International Charter: Lessons learned from the 2011 US Midwestern Floods," *Space Policy*, vol. 42, pp. 54–61, Nov. 2017, doi: 10.1016/j.spacepol.2017.08.003.

[10] S. Voigt *et al.*, "Global trends in satellite-based emergency mapping," *Science (1979)*, vol. 353, no. 6296, pp. 247–252, Jul. 2016, doi: 10.1126/science.aad8728.

[11] J. Rolla *et al.*, "Satellite-Aided Disaster Response," *AGU Advances*, vol. 6, no. 1, Feb. 2025, doi: 10.1029/2024AV001395.

[12] S. Hajji *et al.*, "Enhancing flood prediction through remote sensing, machine learning, and Google Earth Engine," *Frontiers in Water*, vol. 7, Mar. 2025, doi: 10.3389/frwa.2025.1514047.

[13] "**I** REMOTE SENSING AND IMAGE INTERPRETATION Seventh Edition."

[14] A. B. Rimba and F. Miura, "Evaluating the Extraction Approaches of Flood Extended Area by Using ALOS-2/PALSAR-2 Images as a Rapid Response to Flood Disaster," *Journal of Geoscience and Environment Protection*, vol. 05, no. 01, pp. 40–61, 2017, doi: 10.4236/gep.2017.51003.

[15] F. T. . Ulaby *et al.*, *Microwave radar and radiometric remote sensing*. The University of Michigan Press, 2014.

[16] J. A. Richards, *Remote Sensing with Imaging Radar*. Berlin, Heidelberg: Springer Berlin Heidelberg, 2009. doi: 10.1007/978-3-642-02020-9.

[17] J. Clerk Maxwell, "A Dynamical Theory of the Electromagnetic Field," london, Jan. 1865. [Online]. Available: http://rstl.royalsocietypublishing.org/

[18] F. T. (Fawwaz T. Ulaby, *Microwave remote sensing : active and passive*, vol. 1. Reading, Mass. : Addison-Wesley Pub. Co., Advanced Book Program/World Science Division, 1981.
[19] F. Foroughnia, S. M. Alfieri, M. Menenti, and R. Lindenbergh, "Evaluation of SAR and Optical Data for Flood Delineation Using Supervised and Unsupervised Classification," *Remote Sens (Basel)*, vol. 14, no. 15, p. 3718, Aug. 2022, doi: 10.3390/rs14153718.
[20] S. K. McFEETERS, "The use of the Normalized Difference Water Index (NDWI) in the delineation of open water features," *Int J Remote Sens*, vol. 17, no. 7, pp. 1425–1432, May 1996, doi: 10.1080/01431169608948714.
[21] H. Xu, "Modification of normalised difference water index (NDWI) to enhance open water features in remotely sensed imagery," *Int J Remote Sens*, vol. 27, no. 14, pp. 3025–3033, Jul. 2006, doi: 10.1080/01431160600589179.
[22] H. Fujita *et al.*, "Realization of matching conditions for high-resolution spectrometers," *Nucl Instrum Methods Phys Res A*, vol. 484, no. 1–3, pp. 17–26, May 2002, doi: 10.1016/S0168-9002(01)01970-2.
[23] A. Ferretti, C. Prati, and F. Rocca, "Analysis of Permanent Scatterers in SAR interferometry," in *IGARSS 2000. IEEE 2000 International Geoscience and Remote Sensing Symposium. Taking the Pulse of the Planet: The Role of Remote Sensing in Managing the Environment. Proceedings (Cat. No.00CH37120)*, IEEE, pp. 761–763. doi: 10.1109/IGARSS.2000.861695.
[24] "https://space.skyrocket.de/doc_sdat/kondor-fka-m-1.htm#:~:text=Kondor,Nation%3A%20Russia ."
[25] "https://www.ursi.org/proceedings/procGA14/papers/ursi_paper1070.pdf#:~:text=%5BPDF%5D%20RISAT,azimuth%20extent%2C%201%20m."
[26] "https://theprint.in/science/isro-successfully-launches-another-spy-in-the-sky-boosts-indias-surveillance-capability/333561/#:~:text=ISRO%20successfully%20launches%20another%20spy,it%20can%20make%20out."
[27] "https://www.eoportal.org/satellite-missions/umbra-sar#:~:text=Umbra%20SAR%20Constellation%20,."
[28] "https://space.elspina.tech/summary-of-commercial-very-high-resolution-satellite-data-beec6031edbc#:~:text=Summary%20of%20commercial%20very%20high,among%20all%20current%20SAR%20images."
[29] "https://spacenews.com/chinese-partnership-to-create-tianxian-sar-satellite-constellation/#:~:text=constellation%20spacenews.com%20%20Hisea,swath%20width%20of%20100."
[30] "https://syntheticaperturereradar.com/sar-satellite-missions/#:~:text=ICEYE%20Finland%20X,Band%203%20meter."
[31] "https://everydayastronaut.com/s-sar-01-long-march-2c/#:~:text=conservancy%2C%20agriculture%2C%20forestry%2C%20among%20others,resolution%20of%20this%20satellite%E2%80%99s%20images."

[32] "https://radars.ac.cn/en/article/doi/10.12000/JR21113#:~:text=...%20radars.ac.cn%20%20GaoFen,resolution%2C%20large%20swath."
[33] "https://www.cloudeo.group/shop/kompsat-5-134#:~:text=KOMPSAT,%3B%20Polarization."
[34] "https://www.sstl.co.uk/getmedia/b315e056-f198-44d8-9ef4-f02fef9a3da1/NovaSAR-Datasheet.pdf#:~:text=2018%20from%20India%20Global%20access,provide%20information%20on%20detected%20ships."
[35] " https://earth.esa.int/eogateway/missions/saocom#:~:text=Orbit%20Period%2C%2097,ESA%20advertises%20the."
[36] " https://cmr.earthdata.nasa.gov/search/concepts/C3315903479-ASF.html#:~:text=ALOS,46%20days%20to%2014."
[37] " https://www.asc-csa.gc.ca/eng/satellites/radarsat/faq.asp#:~:text=,return%20over%20a%20given%20point."
[38] " https://www.sciencedirect.com/topics/earth-and-planetary-sciences/radarsat#:~:text=Radarsat%20,beam%20mode%2C%20the."
[39] "https://en.wikipedia.org/wiki/COSMO-SkyMed#:~:text=There%20are%20two%20Spotlight%20modes%3A."
[40] " https://airbusus.com/wp-content/uploads/2020/06/r459_9_20171004_tsxx-airbusds-ma-0009_tsx-productguide_i2.01.pdf#:~:text=Defense%20airbusus,m%20resolution%20in%20High%20Resolution."
[41] "https://www.eoportal.org/satellite-missions/copernicus-sentinel-1#:~:text=With%20both%20satellites%20operating%2C%20the,."
[42] "BlackSky Satellite Information Source: https://www.blacksky.com."
[43] "JAXA ALOS-2 Mission Overview Source: https://global.jaxa.jp/projects/sat/alos2/."
[44] "Satellogic Constellation Source: https://satellogic.com/."
[45] "Maxar Technologies – WorldView Satellites Source: https://www.maxar.com/constellation."
[46] "Planet Labs Official Satellite Information Source: https://www.planet.com/products/planet-imagery/."
[47] "Copernicus Open Access Hub (Sentinel missions) Source: https://scihub.copernicus.eu/."
[48] "USGS Landsat Missions Overview Source: https://www.usgs.gov/landsat-missions."
[49] "NASA Earthdata Satellite Missions Source: https://earthdata.nasa.gov/learn/find-data/near-real-time."
[50] https://earth.esa.int/eogateway, "ESA Earth Observation Portal Source https://earth.esa.int/eogateway."
[51] D. Notti, D. Giordan, F. Caló, A. Pepe, F. Zucca, and J. P. Galve, "Potential and Limitations of Open Satellite Data for Flood Mapping," *Remote Sens (Basel)*, vol. 10, no. 11, p. 1673, Oct. 2018, doi: 10.3390/rs10111673.

[52] J. G. Masek *et al.*, “Landsat 9: Empowering open science and applications through continuity,” *Remote Sens Environ*, vol. 248, p. 111968, Oct. 2020, doi: 10.1016/j.rse.2020.111968.
[53] “Landsat Data Continuity Mission.” [Online]. Available: http://earthexplorer.usgs.gov
[54] N. Aeronautics and S. Administration, “Landsat 9 Mission Brochure.” [Online]. Available: https://www.usgs.
[55] “https://docs.planet.com/data/imagery/skysat/.”
[56] M. Drusch *et al.*, “Sentinel-2: ESA’s Optical High-Resolution Mission for GMES Operational Services,” *Remote Sens Environ*, vol. 120, pp. 25–36, May 2012, doi: 10.1016/j.rse.2011.11.026.
[57] “Sentinel-2 Bands.”
[58] A. Tarpanelli, A. C. Mondini, and S. Camici, “Effectiveness of Sentinel-1 and Sentinel-2 for flood detection assessment in Europe,” *Natural Hazards and Earth System Sciences*, vol. 22, no. 8, pp. 2473–2489, Aug. 2022, doi: 10.5194/nhess-22-2473-2022.
[59] “Annual activity report 2020 - Joint Research Centre: https://commission.europa.eu/publications/annual-activity-report-2020-joint-research-centre_en.”
[60] A. Ajmar, P. Boccardo, M. Broglia, J. Kucera, F. Giulio-Tonolo, and A. Wania, “Response to Flood Events,” 2017, pp. 211–228. doi: 10.1002/9781119217930.ch14.
[61] “The Copernicus Emergency Management Service.” [Online]. Available: https://emergency.copernicus.eu/
[62] A. Wania, I. Joubert-Boitat, F. Dottori, M. Kalas, and P. Salamon, “Increasing Timeliness of Satellite-Based Flood Mapping Using Early Warning Systems in the Copernicus Emergency Management Service,” *Remote Sens (Basel)*, vol. 13, no. 11, p. 2114, May 2021, doi: 10.3390/rs13112114.
[63] J. Teng *et al.*, “A Comprehensive Assessment of Floodwater Depth Estimation Models in Semiarid Regions,” *Water Resour Res*, vol. 58, no. 11, Nov. 2022, doi: 10.1029/2022WR032031.
[64] S. Cohen *et al.*, “Sensitivity of Remote Sensing Floodwater Depth Calculation to Boundary Filtering and Digital Elevation Model Selections,” *Remote Sens (Basel)*, vol. 14, no. 21, p. 5313, Oct. 2022, doi: 10.3390/rs14215313.
[65] A. Betterle and P. Salamon, “Water depth estimate and flood extent enhancement for satellite-based inundation maps,” *Natural Hazards and Earth System Sciences*, vol. 24, no. 8, pp. 2817–2836, Aug. 2024, doi: 10.5194/nhess-24-2817-2024.
[66] P. Yousefi, H. A. Jalab, R. W. Ibrahim, N. F. Mohd Noor, M. N. Ayub, and A. Gani, “WATER-BODY SEGMENTATION IN SATELLITE IMAGERY APPLYING MODIFIED KERNEL KMEANS,” *Malaysian Journal of Computer Science*, vol. 31, no. 2, pp. 143–154, Apr. 2018, doi: 10.22452/mjcs.vol31no2.4.
[67] R. G. Congalton and K. Green, *Assessing the Accuracy of Remotely Sensed Data*. CRC Press, 2019. doi: 10.1201/9780429052729.
[68] G. M. Foody, “Status of land cover classification accuracy assessment,” *Remote Sens Environ*, vol. 80, no. 1, pp. 185–201, Apr. 2002, doi: 10.1016/S0034-4257(01)00295-4.

[69] C. S. Arvind, A. Vanjare, S. N. Omkar, J. Senthilnath, V. Mani, and P. G. Diwakar, “Flood Assessment using Multi-temporal Modis Satellite Images,” *Procedia Comput Sci*, vol. 89, pp. 575–586, 2016, doi: 10.1016/j.procs.2016.06.017.
[70] H. Xu and A. Woodley, “Ensemble Learning for Urban Flood Segmentation Through the Fusion of Multi-Spectral Satellite Data with Water Spectral Indices Using Row-Wise Cross Attention,” *Remote Sens (Basel)*, vol. 17, no. 1, p. 90, Dec. 2024, doi: 10.3390/rs17010090.
[71] Y. Shao and R. S. Lunetta, “Comparison of support vector machine, neural network, and CART algorithms for the land-cover classification using limited training data points,” *ISPRS Journal of Photogrammetry and Remote Sensing*, vol. 70, pp. 78–87, Jun. 2012, doi: 10.1016/j.isprsjprs.2012.04.001.
[72] Hossein-Taherijafari, “Hossein-Taherijafari. (2025). GitHub.https://github.com/HTaheriJ?tab=repositories.”